AGU PUBLICATIONS

Water Resources Research

RESEARCH ARTICLE
10.1002/2014WR016826

Key Points:
- Evaluation of teleconnection indices as predictors of lagged seasonal streamflow
- October snow advance index as main predictor of following winter streamflow
- Skills in autumn and spring streamflow forecasting with two seasons in advance

Correspondence to:
J. M. Hidalgo Muñoz,
jhidalgo@ugr.es

Citation:
Hidalgo-Muñoz, J. M., S. R. Gámiz-Fortis, Y. Castro-Díez, D. Argüeso, and M. J. Esteban-Parra (2015), Long-range seasonal streamflow forecasting over the Iberian Peninsula using large-scale atmospheric and oceanic information, *Water Resour. Res.*, *51*, 3543–3567, doi:10.1002/2014WR016826.

Received 2 JAN 2015
Accepted 3 APR 2015
Accepted article online 8 APR 2015
Published online 15 MAY 2015

Long-range seasonal streamflow forecasting over the Iberian Peninsula using large-scale atmospheric and oceanic information

J. M. Hidalgo-Muñoz[1], S. R. Gámiz-Fortis[1], Y. Castro-Díez[1], D. Argüeso[2], and M. J. Esteban-Parra[1]

[1]Department of Applied Physics, Faculty of Sciences, University of Granada, Granada, Spain, [2]Climate Change Research Centre, University of New South Wales, Sydney, NSW 2052, Australia

Abstract Identifying the relationship between large-scale climate signals and seasonal streamflow may provide a valuable tool for long-range seasonal forecasting in regions under water stress, such as the Iberian Peninsula (IP). The skill of the main teleconnection indices as predictors of seasonal streamflow in the IP was evaluated. The streamflow database used was composed of 382 stations, covering the period 1975–2008. Predictions were made using a leave-one-out cross-validation approach based on multiple linear regression, combining Variance Inflation Factor and Stepwise Backward selection to avoid multicollinearity and select the best subset of predictors. Predictions were made for four forecasting scenarios, from one to four seasons in advance. The correlation coefficient (RHO), Root Mean Square Error Skill Score (RMSESS), and the Gerrity Skill Score (GSS) were used to evaluate the forecasting skill. For autumn streamflow, good forecasting skill (RHO>0.5, RMSESS>20%, GSS>0.4) was found for a third of the stations located in the Mediterranean Andalusian Basin, the North Atlantic Oscillation of the previous winter being the main predictor. Also, fair forecasting skill (RHO>0.44, RMSESS>10%, GSS>0.2) was found in stations in the north-western IP (16 of these located in the Douro and Tagus Basins) with two seasons in advance. For winter streamflow, fair forecasting skill was found for one season in advance in 168 stations, with the Snow Advance Index as the main predictor. Finally, forecasting was poorer for spring streamflow than for autumn and winter, since only 16 stations showed fair forecasting skill in with one season in advance, particularly in north-western of IP.

1. Introduction

Water-resource management has been an important subject in the Iberian Peninsula (IP) for many decades, particularly since the second half of the 20th century, with the development of major irrigation and hydropower systems. Natural water resources in the IP are used intensively, especially in agriculture, but also in other sectors, such as hydropower industry or tourism.

Together with the increase in water demand, the observed decrease in water availability has intensified the situation of water stress in the IP. *López-Moreno et al*. [2009] found that the Portuguese part of the Tagus River Basin has undergone more severe droughts than has the upstream part, in terms of both magnitude and duration, because of the reservoir construction. Also, it has been found a marked reduction in annual, winter, and spring streamflows in most of the Iberian subbasins, especially in the south [*Lorenzo-Lacruz et al*., 2013a], and a trend toward increased streamflow drought severity in the majority of the regions [*Lorenzo-Lacruz et al*., 2013b]. In agreement with this, *Vicente-Serrano et al*. [2014] found that hydrological drought frequency and severity have also increased in the past five decades in natural, regulated, and highly regulated basins. The observed decrease in water-resource availability in the Mediterranean Basin is also expected to continue in the future. In this regard, an ensemble of regional climate models driven by several GCMs using the A1B scenario (used in support of the AR4 IPCC) project a robust decrease in runoff after 2050 [*Sánchez-Gómez et al*., 2009].

Taking into account, the observed and postulated changes in water resources, particularly in the Mediterranean region, maximizing water-management efficiency is key to water-resource management and planning. The study of variability in river flows rather than other variables such as precipitation when planning water-management strategies seems to be more appropriate since the hydrological system acts as spatial and

temporal integrator of precipitation (rain and snow), temperature, and related evapotranspiration over a specific region. Variations in these fields are amplified in streamflow and, in general, it is easier to detect a change in discharge than directly in the basic climatic variables [*Dettinger and Diaz*, 2000; *Trigo et al*., 2004]. Long-term forecasting based on monthly, seasonal, or annual time scales is very useful in reservoir operations and irrigation-management decisions, protection of the environment, or in the reduction of expenses in flood and drought mitigation. Furthermore, management decisions for operating river diversions and dams are made early in the year in anticipation of the forthcoming seasonal streamflows. Consequently, interest in long-range predictability of river discharge variability, especially those that use as predictors the information provided by the variability of sea surface temperature or atmospheric pressure, has markedly increased worldwide in recent years, as for example for North America [*Lamb et al*., 2010; *Oubeidillah et al*., 2011; *Tang et al*., 2011; *Kalra et al*., 2013], South America [*Gutiérrez and Dracup*, 2001; *Tootle et al*., 2008], Europe [*Ionita et al*., 2008, 2011; *Gámiz-Fortis et al*., 2010, 2011; Aziz et al., 2012], Asia [*Chandimala and Zubair*, 2007], Africa [*Sittichok et al*., 2014], or Australia [*Piechota et al*., 2001; *Chiew et al*., 2003].

Regarding the IP, *Gámiz-Fortis et al*. [2008a] examined the interannual variability and predictability of the winter streamflow of the main IP international rivers (Douro, Tagus, and Guadiana) for the period 1923–2004, by applying autoregressive-moving-average (ARMA) models to the Singular Spectrum Analysis (SSA) filtered streamflow. Additionally, *Gámiz-Fortis et al*. [2008b] analyzed the role of the Atlantic summer and autumn sea surface temperatures (SSTs) on the predictability of these winter IP River flows. A similar approach, combining the predictability skill of SST in seasonal and interannual streamflow variability with the knowledge of main oscillatory modes of variability presented in streamflow time series, was used to investigate the predictability of the Douro [*Gámiz-Fortis et al*., 2010], Ebro [*Gámiz-Fortis et al*., 2011], and Internal Catalonian Basins streamflow [*Hernández-Martínez et al*., 2014]. Overall, these studies center their attention in a particular river basin or gauge station, being representative of a particular catchment area, and refining the methodologies to obtain the better possible predictions. Also, usually they are limited to a specific season.

The approach followed in this paper complements the previous studies, since the main goals comprise an analysis of the forecasting skill of the main modes of climate variability, commonly referred as teleconnection patterns [*Barnston and Livezey*, 1987; *Hurrell et al*., 2003; *Quadrelli and Wallace*, 2004], over streamflow in the IP rivers in subsequent seasons. To this end, a large streamflow database covering most of the IP is used instead some individual stations and the study is not restricted to a particular season. In particular, it identifies which of the large-scale variability modes affect seasonal streamflow in the IP in the following seasons. Subsequently, information is provided concerning the ability to predict seasonal (autumn, winter, and spring) streamflow in the IP based on the previously identified climatic predictors. In this procedure, four forecasting scenarios are established, considering up to four different lags between predictors and predictands, which provide predictions of seasonal streamflow from one year in advance, with seasonal updates until the season prior to the forecasted one.

This paper is structured as follows: section 2 presents the main climatic characteristic of the region and data used. Section 3 explains the methodology developed for forecasting purposes. The results are presented in section 4, discussion in section 5, and the conclusions in section 6.

2. Data

2.1. Study Area

The IP is located between 36°N–44°N and 3°E–10°W (Figure 1). According to Köppen climate classification, the climatic regimes in the IP are: temperate climate, such as Csa (temperate with dry or hot summer, over the majority of the southern-central plateau region, and the Mediterranean coastal regions, except the arid zones in the southeast), Cfa (temperate with a dry season and hot summer, mainly in the northeast, within an area of medium altitude which surrounds the Pyrenees and the Iberian mountains), or Cfb (temperate with a dry season and temperate summer, in the Cantabrian mountains, in the Iberian mountain ranges, as well as part of the northern central plateau region and a large part of the Pyrenees, except areas of high altitude), dry climates, such as Bsk (in the southeast of the IP) and also cold climates in the mountains. A more detailed definition of the IP climates can be found in [*AEMET*, 2011]. The main factors affecting the climate of the IP are its location, in midlatitudes of the Northern Hemisphere (NH), the influence of the Atlantic

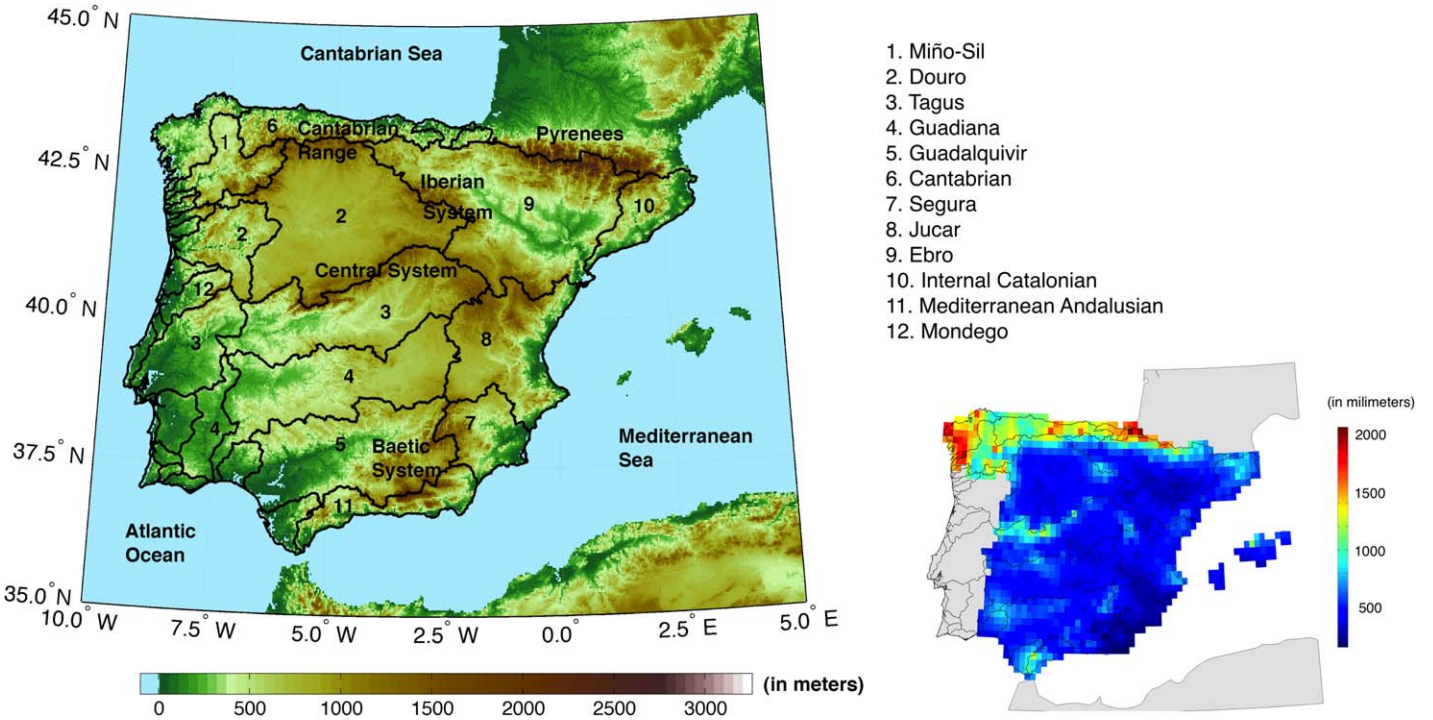

Figure 1. Geographical features of the Iberian Peninsula and identification of the main river basins; the Douro, Tagus, and Guadiana basins are separated into two parts by a line according their location in Portugal or Spain. In the right bottom corner, it is shown the mean annual precipitation through the period 1975/2007 across Spain, calculated using the Spain02 data set developed by *Herrera et al*. [2012].

Ocean and the Mediterranean Sea and its rugged terrain, with the mountain ranges acting as barriers and passageways that determine local climates. These factors generate a northwest-southeast gradient in annual precipitation distribution, varying from more than 2000 mm/yr in the northwest to less than 300 mm/yr in the southeast (Figure 1, right). The large-scale precipitation is modulated primarily by the position of the Azores anticyclone that acts as a blocking structure in the summer, pyrreventing the low-pressure systems from reaching the IP, and bringing hot and dry weather. The scarce summer precipitation is due mostly to local factors and convective storms [*Serrano et al*., 1999]. On the contrary, winter months account about 40% of annual precipitation. In winter, the Azores High moves toward the tropics accompanied by a southward displacement of the jet-stream, allowing the low-pressure systems to enter the IP, resulting in wetter conditions. Note that in the eastern part of the IP, mesoscale convective systems are also responsible for high rainfall rates, especially in transient seasons [*García-Herrera et al*., 2005; *Paredes et al*., 2006].

The river system in the IP presents a great variability of seasonal and annual flows [*Iglesias et al*., 2007; *Lorenzo-Lacruz et al*., 2010] as a consequence of the high spatiotemporal variability of precipitation [*Esteban-Parra et al*., 1998] and a diverse environment. River basins (Figure 1) in northern sector of Atlantic watershed present higher mean annual flow (10,570 hm^3/yr for the Miño Basin, 13,788 hm^3/yr for the Douro Basin, 1240 hm^3/yr for the Mondego Basin, and 12,350 hm^3/yr for the Tagus River) than do rivers in the southern sector of Atlantic watershed (4039 hm^3/yr for the Guadiana River and 3780 hm^3/yr for the Guadalquivir River), and greater than do rivers in the Mediterranean Basins (600 hm^3/yr for the Mediterranean Andalusian Basin, 118 hm^3/yr for the Segura Basin, 1023 hm^3/yr for the Jucar Basin, and 779 hm^3/yr for the Internal Catalonian Basins). The exception is the Ebro Basin, which has an abundant flow (12,279 hm^3/), generated in the Cantabrian Range and in the Pyrenees.

2.2. Streamflow Data and Quality Control

Monthly streamflow time series of gauging stations in each river basin were established from the following water agencies: Centro de Estudios Hidrográficos (CEDEX), Agència Catalana de l'Aigua, Agencia Andaluza del Agua, and Sistema Nacional de Informaçao de Recursos Hídricos (SNIRH) of Portugal.

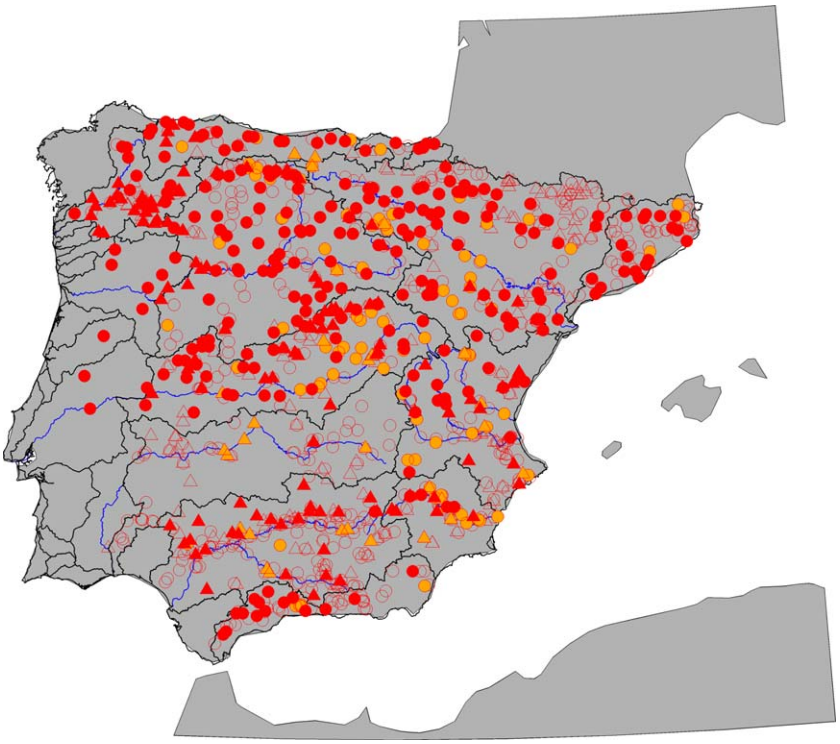

Figure 2. Filled in red, the 382 stations that pass the quality control. Filled in orange, the 122 stations considered as no homogeneous. Unfilled, the remaining stations until the 1380 total original database. Circles and triangles represent gauging stations located in the mainstreams of rivers and reservoirs, respectively.

The data set compiled represents 808 gauge stations in Spain, 246 in Portugal, and 326 reservoir entrances in Spain, totaling 1380 data series (Figure 2). The length and quality of these series are highly variable. We evaluated the number and spatial density of available stations for different periods and percentage of missing values, taking into account that in climate studies it is advisable to use records longer than 30 years. After this evaluation, we concluded that the period with the highest number of stations (and with the best spatial distribution) and less than 10% of missing values spanned October 1975 to September 2008 (a time period defined in terms of hydrological years instead of natural years). As a result, a total of 504 from the original 1380 stations surpass these criteria.

Subsequently, monthly streamflow time series were seasonally averaged. Often, in climate studies, seasons are defined as: winter (December–February, DJF), spring (March–May, MAM), summer (June–August, JJA), and autumn (September–November, SON). However, the components of the hydrological cycle interact in multiple ways in a catchment, which introduces time lags between a decline in precipitation and when this becomes evident in other components of the hydrological cycle [*Vicente-Serrano and López-Moreno*, 2005; *Lorenzo-Lacruz et al*., 2010]. Thus, it is reasonable to consider a possible lag response of streamflow with respect to precipitation. Accordingly, *Trigo et al*. [2004] studied the response of precipitation and streamflow in the IP to the NAO and found that, whereas DJF precipitation is well related to DJF NAO, the JFM mean river flow proved to be more closely associated with the 1 month leading (DJF) NAO index than was the simultaneous (DJF) river flow. Also, we evaluated the month-to-month streamflow correlation, finding that March–April correlation presented lower values than most of the month-to-month correlations. Consequently, we grouped March with February and January defining winter as JFM. As a result, the spring was defined as April–June (AMJ), summer from July to September (JAS), and autumn from October to December (OND).

Once the seasonal streamflow time series were averaged, we analyzed their quality, in order to discard those series with a nonhomogeneous behavior. The main cause of inhomogeneity on streamflow time series in the IP is the degree of regulation to which the main IP Rivers are subjected. The situation of recurrent water stress in the IP, together with the increasing drought frequency since the 1970s [*Iglesias et al*.,

2007; *Vicente-Serrano*, 2006], have resulted in the construction of a complex network of dams and channels to optimize the use of available water resources, especially in the second half of 20th century, leading to modifications in the natural regime of some rivers.

To address the homogeneity of streamflow time series, the nonparametric Pettitt test [*Pettitt*, 1979] was used together with a measure of the degree of alteration in the intra-annual regime as a consequence of the possible break points detected by Petittt test (see Appendix A for further details).

As a result, 122 stations of the original 504 were discarded and the final database composed of 382 stations was considered homogeneous and covering 1975–2008 with less than 10% of missing values (Figure 2). Thereafter, the missing values were filled in using a linear-regression approach. The station showing the highest correlation with the predictand was used as the predictor (in most cases correlation values were above 0.8). If no predictor was identified, missing values were filled in using the seasonal mean value.

Regarding the intra-annual streamflow variability, most of the stations, especially those located in the central and western IP, present their maximum discharge during winter. Some stations located in the proximities of the Pyrenees and Iberian System mountain ranges have their maximum flow levels during spring, as a result of snowmelt. Other stations on the Mediterranean slope have their greatest streamflow values in autumn, as a consequence of the influence of the orography and convective precipitation events during late summer and early autumn. The minimum values and variability of river discharge are found in summer. Accordingly, this study focuses on the evaluation of autumn, winter, and spring streamflow predictability.

Hydrological series commonly do not follow a normal distribution, being highly skewed. Additionally, the magnitude of the monthly streamflow values varies greatly among the stations, because of the great difference in climatic areas, and the location of stations in a particular basin (in the mouth of the river, in the headwaters, or a particular tributary). To make the magnitudes between all stations comparable, we standardized the time series. Some studies concerning streamflow variability of IP rivers have used different distributions to fit the streamflow time series, such as Pearson type 3 [*Vicente-Serrano*, 2006; *Gámiz-Fortis et al*., 2010; *Lorenzo-Lacruz et al*., 2010], lognormal [*Gámiz-Fortis et al*., 2011], or Generalized Pareto [*Hernández-Martínez et al*., 2014]. The present study followed an approach similar to the one proposed in *Vicente-Serrano et al*. [2011]. These authors selected the most appropriate distribution for each time series between a subset of three parametric distributions commonly used in hydrology. The Generalized Extreme Value, Generalized Pareto, Generalized Logistic, Pearson-type 3, and the three parameters lognormal distributions were evaluated. The L-moments approach has been used to fit the parameters and select the most suitable distribution in each case. Once it was determined which distribution of probability was the most suitable, seasonal streamflow time series were standardized. In addition, the Lilliefors test [*Lilliefors*, 1967] was applied to the standardized time series to check their normality. Results indicated that between 90% and 94% (depending on the season) of the standardized time series follow a normal distribution with a 95% of confidence level.

2.3. Teleconnection Indices

Two of the most important teleconnection patterns are El Niño/Southern Oscillation (ENSO) and the North Atlantic Oscillation (NAO). The NAO is the most prominent and recurring extratropical teleconnection pattern in the NH. Generally, the NAO refers to the meridional seesaw, or the dipole structure, typically associated with the north center near Iceland and the south center near the Azores of the SLP field. The negative phase of the NAO causes changes in the direction of westerlies that bring moist air over the IP and above normal precipitation. The importance of winter NAO as the major atmospheric mechanism controlling the precipitation during wintertime in the central and western IP has been described by several authors [i.e., *Rodó et al*., 1997; *Rodríguez-Puebla et al*., 1998; *González-Rouco et al*., 2000; *Trigo and Palutikof*, 2001]. Also, effects of NAO on winter streamflow in Iberian Rivers have been identified [*Trigo et al*., 2004; *López-Moreno et al*., 2007; *Lorenzo-Lacruz et al*., 2011; *Morán-Tejeda et al*., 2011].

The ENSO encompasses two linked phenomena, a quasiperiodic warming in the tropical Pacific near South America and an adhering effect, and the zonal anomaly of Sea Level Pressure (SLP) in the tropical Pacific (the Southern Oscillation). The ENSO -SST variability is strongest in the Pacific Ocean but extends to the tropical Atlantic and Indian Oceans with systematic lags of one to three seasons [*Mestas-Nuñez and Enfield*, 2001]. Several studies have shown significant relationships between ENSO events and precipitation or

streamflow variability at the global scale [*Dettinger and Diaz*, 2000; *Chiew and McMahon*, 2002], for the European area [*Mariotti et al*., 2002; *García-Serrano et al*., 2011; *Shaman and Tziperman*, 2011] and, particularly for the IP [*Rodó et al*., 1997; *Pozo-Vázquez et al*., 2005; *Lorenzo et al*., 2010; *Vicente-Serrano et al*., 2011]. So, for southern Europe and during La Niña events, a statistically significant precipitation anomaly pattern with negative anomalies, resembling the precipitation pattern associated with the positive phase of the NAO is found. There are other teleconnection patterns that account for an important percentage of the climatic variability and have an influence on IP climate. For example, *Rodríguez-Puebla et al*. [2001] studied the influence of North Atlantic Oscillation (NAO), East-Atlantic (EA), the East-Atlantic/Western-Russia (EA-WR), and the Polar/Eurasian (POL) patterns on winter precipitation in the IP. In addition, it has been found that the EA and EA-WR patterns represent a significant contribution for the precipitation over the northern IP [*Sáenz et al*., 2001] as well as parts of the eastern Mediterranean area [*Xoplaki et al*., 2004; *Krichak et al*., 2002]. *de Castro et al*. [2006] found a significant contribution of the NAO and also Scandinavian (SCAND), EA-WR, and EA patterns in explaining the main variability of precipitation and river-flow regimes in Galicia (north-west of IP). *Casanueva et al*. [2014] examined the relationship between the variability of extreme precipitations events in Europe and different teleconnection patterns, such as the Arctic Oscillation (AO), NAO, SCAND, EA, EA-WR, the Southern Oscillation Index (SOI), the Atlantic Multidecadal Oscillation (AMO), and the Madden-Julian Oscillation (MJO). Overall, the results of these studies show for winter precipitation in the IP positive significant correlations with the EA in the western Iberia, and negative correlations with the EA-WR for the northern part. The Western Mediterranean Oscillation (WeMO) [*Martin-Vide and Lopez-Bustins*, 2006] has been related to precipitation episodes in the Mediterranean area of IP [*Lopez-Bustins et al*., 2008; *Martin-Vide et al*., 2008; *Hidalgo-Muñoz et al*., 2011] and with IP river discharge [*Lorenzo-Lacruz et al*., 2013a], showing significant negative correlations.

In recent years, it has been observed an increase in studies concerning the influence of the Siberian snow-cover variability in autumn in the climate of the NH during the following winter [*Bojariu and Gimeno*, 2003; *Cohen and Saito*, 2003; *Saito and Cohen*, 2003; *Cohen et al*., 2007], particularly its connection to the winter phase of the Arctic Oscillation (AO). In this regard, a new index, the Snow Advance Index (SAI), has been defined as a measure of how rapidly the Eurasian snow cover increases in October, which affects winter atmospheric conditions in the NH through the strength and position of the Siberian High (more details about the conceptual model can be found in *Cohen and Jones* [2011]). This standardized index, computed by the regression coefficient of the least square fit of Eurasian snow-cover extension during October equatorward of 60°N, has been proposed as a potential predictor of the following winter AO [*Cohen and Jones*, 2011]. There are two versions of the SAI, one calculated using weekly data of snow cover that covered the period from October 1972 to October 2010, and another one calculated as the regression coefficient using daily data of the extent of snow cover which is available since 1997. The second version shows higher correlation with the winter climate of the IP [*Brands et al*., 2012, 2014], which has been also confirmed here for the winter streamflow (not shown). In order to take advantage of this, a new SAI index was created for this studio, using the data of SAI calculated using daily snow cover measures and completing the rest of the years (1974–1996) with the SAI calculated using the weekly snow cover data. Note that it was checked that the new index presents zero mean and one unit of standard deviation and the time series does not present inhomogeneity.

In addition to these commonly used teleconnection indices, others related to the North Atlantic climate have been examined in this paper. The North Pacific has also been hypothesized to influence decadal variations in different geographical regions, through the Pacific Decadal Oscillation (PDO) [*Tomita et al*., 2001]. Particularly, the teleconnection between the PDO and rivers in Europe has been investigated by various authors [*Dettinger and Diaz*, 2000; *Rimbu et al*., 2002; *Bardin and Voskresenskaya*, 2007; *Gámiz-Fortis et al*., 2011]. Also, The Pacific North Atlantic (PNA) has been proposed as one of the links between the tropical forcing and the extratropical circulation response in the North Atlantic area [*Pozo-Vázquez et al*., 2005]. In addition to these indices, the ability of other patterns related to the North Pacific Ocean, such as the Western Pacific pattern (WP), the East Pacific-North Pacific pattern (EP-NP), and the North Pacific Gyre Oscillation (NPGO) [*Di Lorenzo et al*., 2008] have been considered in this study. Also, the Indian Ocean has been identified as possibly modulating ENSO variability through an extension of the Walker Circulation to the west and associated flow of warm tropical ocean water from the Pacific into the Indian Ocean [e.g., *Izumo et al*., 2010; *Frauen and Dommenget*, 2012]. The potential influence of the Indian Ocean on IP climate, especially over

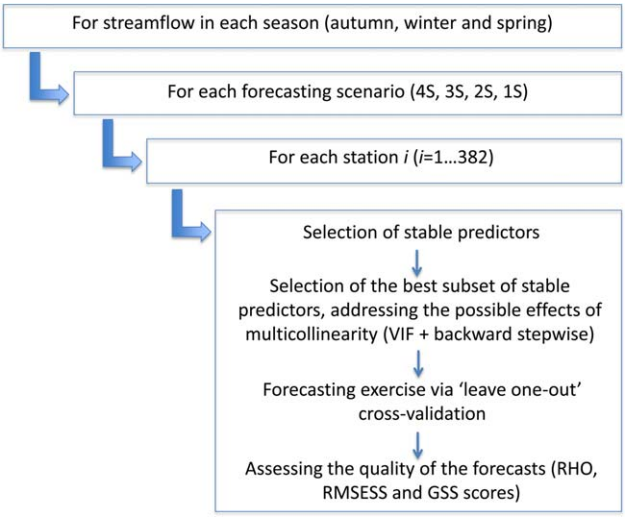

Figure 3. Workflow showing the methodology steps followed in the forecasting procedure.

river-flow variability, has been pointed out [*Hernández-Martínez et al.*, 2014]. Here, we used the Indian Ocean Dipole (IOD), a western-eastern dipole of sea surface temperature differences in the Indian Ocean, in order to evaluate the teleconnection with Indian Ocean. Finally, the Atlantic Multidecadal Oscillation (AMO) was included, which has also been related to streamflow variability in France [*Aziz et al.*, 2011].

In summary, the set of teleconnection indices explored as predictors included: The monthly time series of Artic Oscillation (AO), North Atlantic Oscillation (NAO), East Atlantic pattern (EA), Pacific/North American pattern (PNA), Western Pacific pattern (WP), East Pacific North Pacific pattern (EP-NP), Scandinavian pattern (SCAND), East Atlantic Western/Russian pattern (EA-WR), Atlantic Multidecadal Oscillation (AMO), El Niño indices (Niño1+2, Niño3, Niño4, Niño3.4), Southern Oscillation Index (SOI), and Pacific Decadal Oscillation (PDO), which were obtained from the Climate Prediction Center (CPC) at the National Center of Environmental Predictions (NCEP; www.cpc.noaa.gov); the monthly time series of El Niño Modoki (EMI) and Indian Ocean Dipole (IOD), obtained from the Japan Agency for Marine-Earth Science and Technology (www.jamstec.go.jp/); the monthly time series of Western Mediterranean Oscillation (WeMO), downloaded from http://www.ub.edu/gc/English/wemo.htm; the time series of the North Pacific Gyre Oscillation (NPGO), from http://www.o3d.org/npgo/; and the time series of Snow Advance Index (SAI), that was kindly provided by J. Jones (personal communication, 2012).

3. Methodology

The procedure followed for making seasonal predictions consists of the establishment of four forecasting scenarios. Each of these refers to the seasons in advance for which the predictions are made. For example, in case of spring streamflow forecast, in the first scenario (referred as "4S" hereafter) the predictions are made four seasons in advance, using the teleconnection indices of the previous spring as predictors. The following scenario ("3S") uses as predictors the teleconnection indices from four to three seasons beforehand, i.e., the teleconnection indices of the previous spring and summer. The next scenario ("2S") uses as predictors the teleconnection indices from four to two seasons beforehand, i.e., the seasonal teleconnection indices of the previous spring, summer, and autumn. The last scenario ("1S") uses as predictors the teleconnection indices from four to one season beforehand, i.e., the teleconnection indices of the previous spring, summer, autumn, and winter. The seasonal teleconnection indices were defined as averages of 3 month periods, autumn (September–November, "son"), winter (December–February, "djf"), spring (March–May, "mam"), and summer (June–August, "jja"). When a "1" is added to these acronyms, it means the season belongs to the year prior to the seasonal streamflow predicted.

The forecasting methodology used here can be summarized in three steps: (1) developing a set of potential predictors based on previous seasonal teleconnection indices, by using correlation stability analysis; (2) building linear-regression models; and (3) assessing the quality of the forecast. Figure 3 shows a workflow summarizing the steps followed in the work.

3.1. Determination of Stable Predictors

We evaluated the stability of the correlation between 77 seasonal teleconnection indices (the four seasonal averages of the 19 teleconnection indices and the SAI, which is measured only in October) and seasonal

streamflow (autumn, winter, and spring) at each gauging station. A seasonal time series corresponding to a teleconnection index was considered a stable predictor if it showed stable teleconnection with at least 20 stations (around 5% of the total) or in case of a lower number, if they are grouped together. To evaluate the stability of the correlations, a similar approach to the one used by *Ionita et al*. [2008] and *Gámiz-Fortis et al*. [2010] was followed. The correlation between seasonal streamflow and teleconnection indices was calculated for 19 moving windows of 15 years (running 1 year). The correlation between predictor and predictand is considered to be strongly stable (stable) when more than 80% of the total 19 moving windows present significant correlations at 95% (90%) level, and no change in correlation signs is shown. Note that the serial correlation was taken into account in determining the critical value for correlation significance. This was done through the calculation of the effective degrees of freedom, according *Bretherton et al*. [1999].

3.2. Building Multiple-Linear-Regression Models

A multiple linear regression analysis was used to model the relationships between predictors and predictands. When a large set of predictors is used to build a regression model, an excessive correlation among explanatory variables (collinearity) can complicate or prevent the identification of an optimal set of explanatory variables for a statistical model. The effect of multicollinearity results in highly variable parameter estimators making it difficult to diagnose the factors that are most important in specifying the model. Furthermore, multicollinearity increases the standard errors of the coefficients, so that coefficients for some independent variables may be found not to be significantly different from 0, whereas without multicollinearity and with lower standard errors, these same coefficients might have been found to be significant and the researcher may not have come to null findings in the first place.

To answer the question about how to address multicollinearity in hydrologic regression models, we follow the recommendations given in *Kroll and Song* [2013], using a simple approach to identify collinearity, the variance inflation factor (VIF), and combining its results in a backward stepwise multiple-linear regression to select the most appropriate set of predictors. Formally, VIF measures how much the variance of the estimated coefficients is increased over the case of no correlation among the predictor variables. The VIF for a single explanatory variable is calculated using the r-squared value of the regression of that variable against all other explanatory variables.

$$VIF_j = \frac{1}{1-R_j^2} \tag{1}$$

where the VIF for variable j is the reciprocal of the inverse of R_j^2, coefficient of determination from a regression of predictor j on the remaining predictors.

When the variation of predictor j is largely explained by a linear combination of the other predictors, R_j^2 is close to 1, and the VIF for that predictor is correspondingly large. The inflation is measured relative to an R_j^2 of 0 (no collinearity), and a VIF of 1. According with the literature [*Hair et al*., 1995], the VIF tolerance level should be below 10 or 5 (R^2 higher than 0.9 or 0.8). In small samples, less than 50 points, a threshold of 5 is preferable [*Zuur et al*., 2010]. If there are two or more variables with a VIF greater than 5, the variable with the highest VIF must be removed, recalculating all VIF values with the new set of variables and repeating the process until all VIF values are below the threshold.

Afterwards, we used a stepwise regression approach which is an iterative semiautomated process of building a model by successively adding or removing variables based on the *F*-statistics of their estimated coefficients. The stepwise option lets us either to start with *no* variables in the model and proceed forwards (adding one variable at a time), or start with all potential variables in the model and proceed backward (removing one variable at a time). We used backward selection in this study.

3.3. Assessing the Quality of the Forecast

To avoid artificial skill effects in forecasting, the leave-one-out cross-validation method is commonly used in small samples. We eliminated a further potential source of dependency/artificial skill by removing the trend and the mean in each step of the cross-validation [*von Storch and Zwiers*, 1999].

Verification measures enabled us to evaluate the quality of the forecast, its weakness, and strengths [*Jolliffe and Stephenson*, 2003]. In this study, the Pearson's correlation coefficient (RHO hereafter), the Root Mean

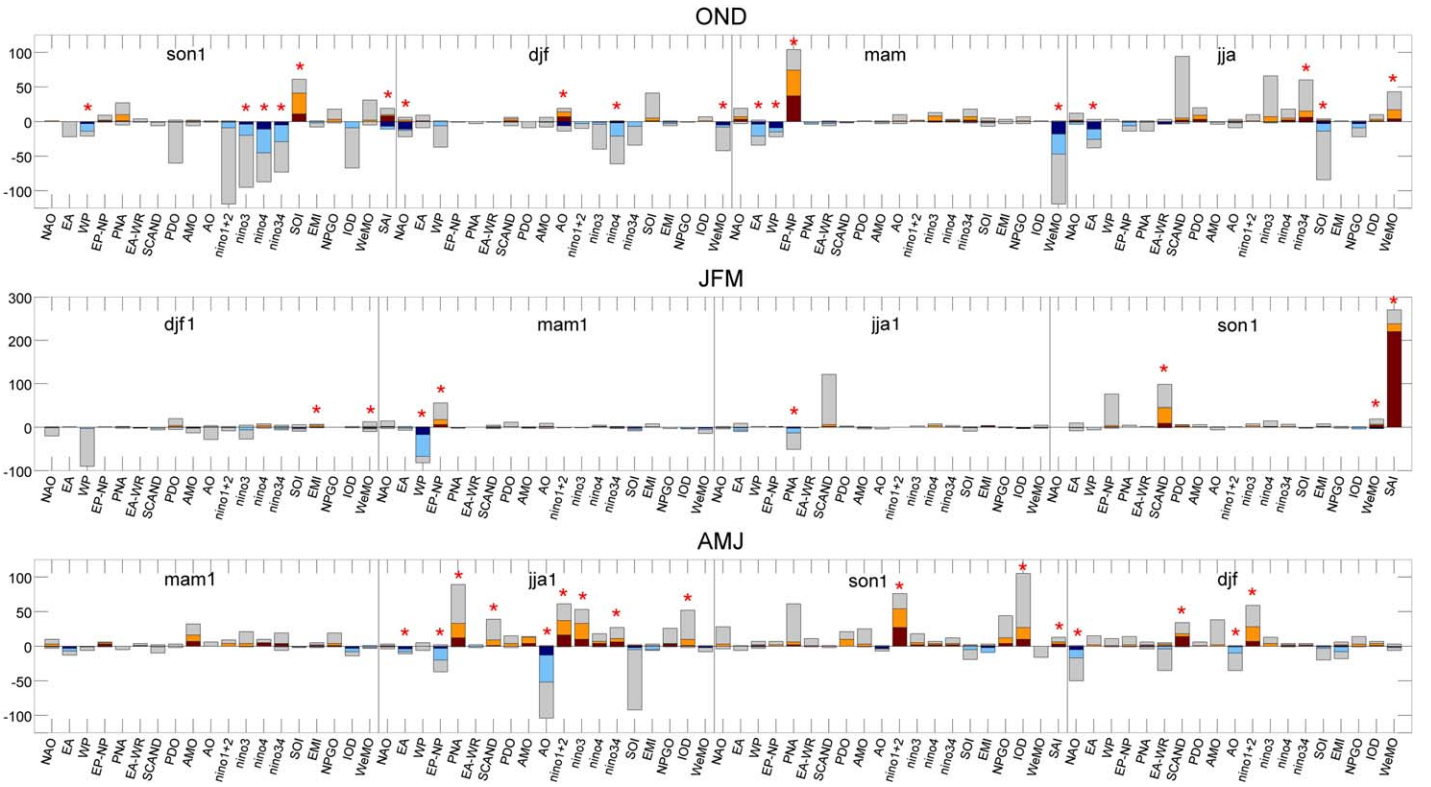

Figure 4. Number of stations that present a significant (at 95% confidence level; in gray bars), stable (light blue and orange bars), and strongly stable (dark blue and dark red bars) correlation between teleconnection indices and lagging seasonal streamflow for autumn (OND) streamflow (top); winter (JFM) streamflow (middle); and spring (AMJ) streamflow (bottom). son1, djf1, mam1, and jja1 correspond to autumn, winter, spring, and summer of the previous year, respectively. Note that negative numbers signify sum of stations with negative correlations. With asterisk those indices that were selected as the potential predictors.

Square Error Skill Score (RMSESS), and the Gerrity Skill Score (GSS) are used. The RHO is a measure of the linear relation. The RMSESS provides a measure of error. It is referenced to the climatology mean, so that positive (negative) values of RMSESS indicate better (worse) forecasting skill than climatological mean. The GSS identifies the accuracy in forecasting streamflow that are in the same category as the observations. To the calculation of GSS, three categories were considered: below normal, normal, and above normal, by the 33rd and 66th terciles.

4. Results

4.1. Identification of Stable Predictors

A summary of the stability of correlations between seasonal streamflow and teleconnection indices is shown in Figure 4. This figure indicates the number of gauging stations that present significant and stable (and also strongly stable) correlations with teleconnection indices corresponding to different seasons. An asterisk indicates the seasonal teleconnection indices that present stable correlations with at least 20 stations (~5% of the total) or, in case of less than 20, if they are grouped together belonging to a basin represented by less than 20 stations in the database used here (such as the Mediterranean Andalusia or the Internal Catalonian Basin). From this figure, it is worth highlighting the large number of stations where the OND streamflow is significantly correlated with ENSO indices of the previous autumn. However, the number of stations where these correlations are stable was lower. This feature (significant but not stable correlations) was also found in correlations between OND streamflow and WeMO in the previous spring and SCAND and SOI in the previous summer. A total of 18 teleconnection indices (those with an asterisk in Figure 4) of the 77 evaluated are considered stable predictors for autumn streamflow. For JFM streamflow, it bears noting that few teleconnection indices (only 8 of the 77 analyzed) were identified as stable predictors (with asterisk in Figure 4). For example, there is a notable number of stations with significant but unstable correlations with WP and SCAND in previous winter and summer, respectively. A remarkable case is that of

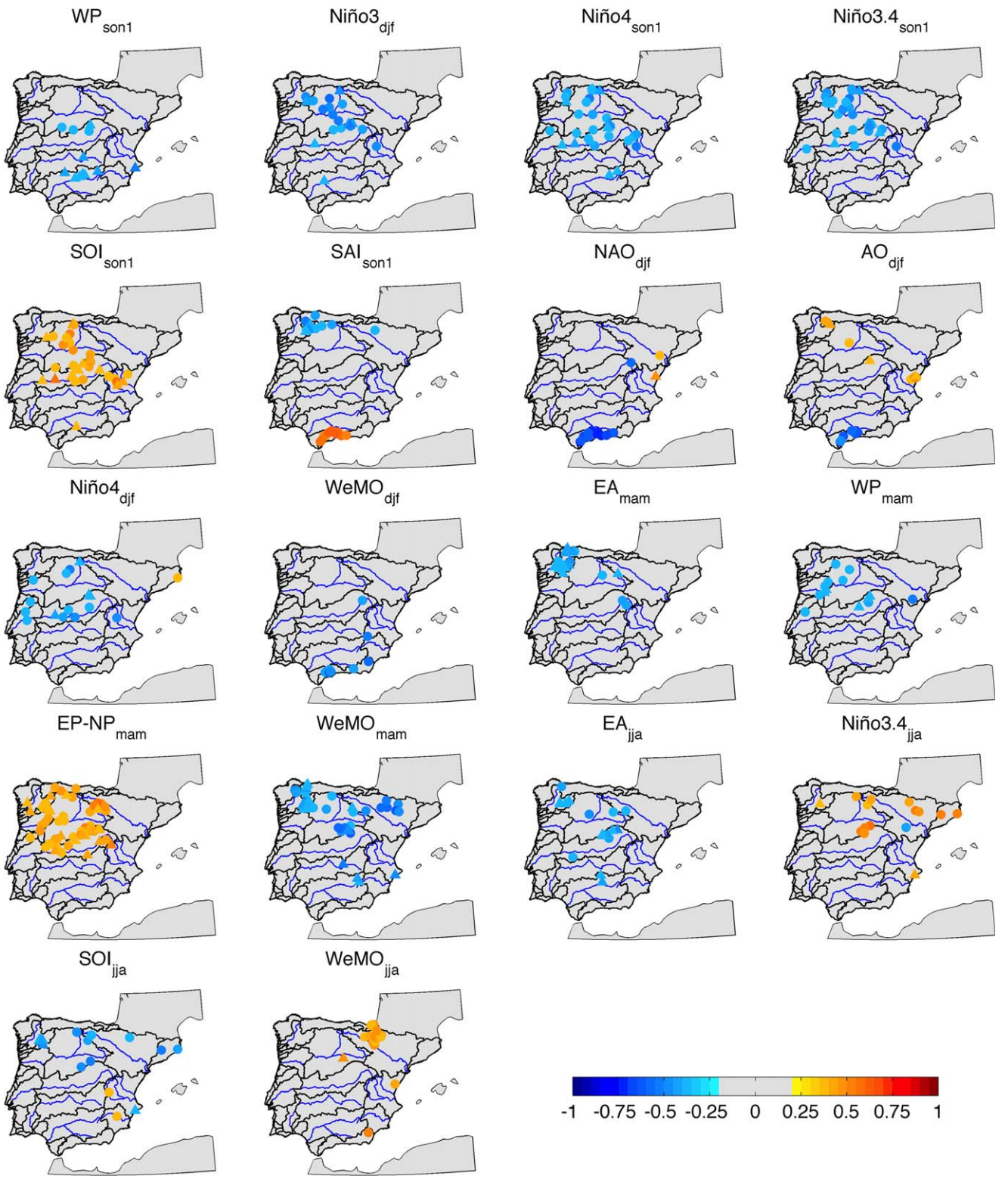

Figure 5. Maps of the correlation between the teleconnection indices selected as predictors and autumn (OND) streamflow. In the title of each map, the acronym of the corresponding teleconnection index and its season (subindex). Only significant and stable correlations are displayed. Circles and triangles represent gauging stations located mainstream of rivers and reservoirs, respectively.

SAI, which was found to be a stable predictor of winter streamflow in 238 stations. In the case of AMJ streamflow, 16 of the 77 seasonal teleconnection indices evaluated were considered stable predictors (with asterisk). Notably, none of the teleconnection indices in the previous spring was considered to be a stable

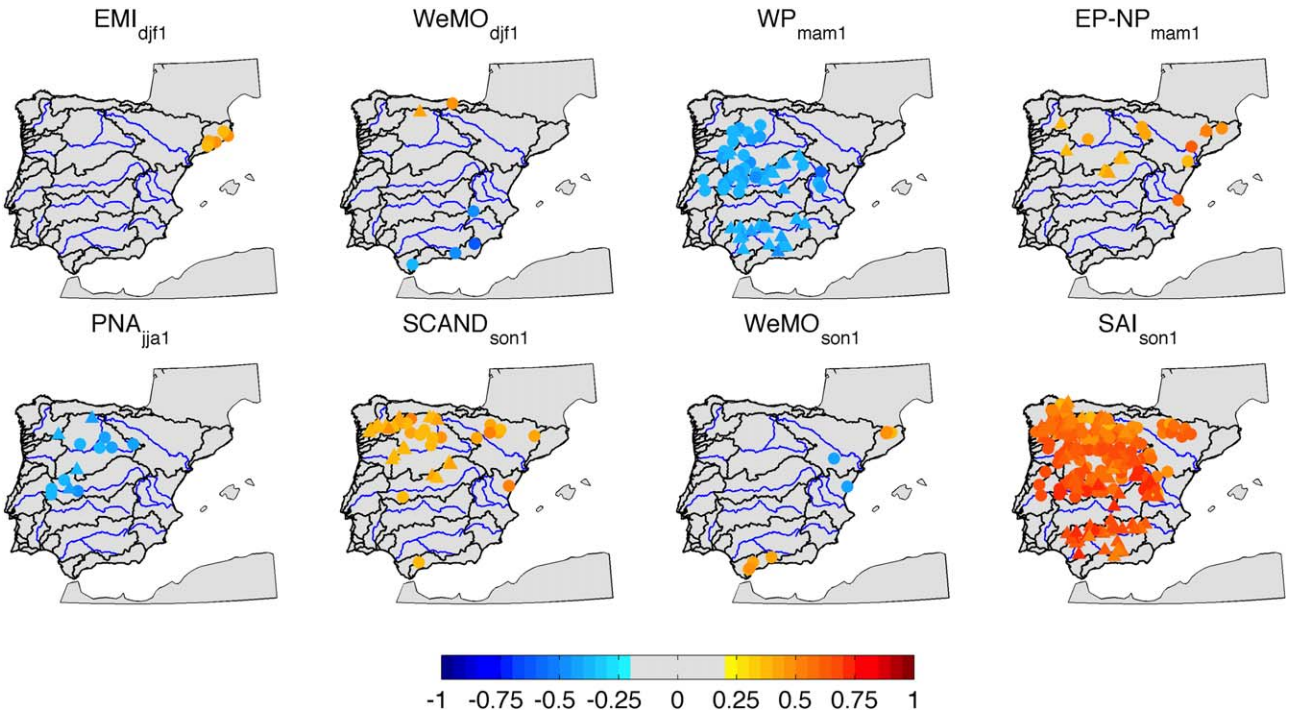

Figure 6. As Figure 5 but for winter (JFM) streamflow.

predictor, most of them being in previous summer. Additionally, significant but unstable correlations appear with SOI in the previous summer.

The correlation maps between stable predictors (with asterisk in Figure 4) and seasonal streamflow are displayed in Figures 5–7 for autumn, winter, and spring, respectively. Regarding the predictors corresponding to the previous autumn (Figure 5), the most relevant is the presence of various indices related to the ENSO phenomenon (Niño3, Niño4, Niño3.4, and SOI). Although with some minor differences, they present stable correlations with stations located in the Douro and Tagus Basins, but also with some stations located in the upper Jucar and Guadalquivir Basin. El Niño4 is the index that presents stable correlation with the largest number of stations (45). These correlations are not high in magnitude (around 0.4 in absolute value). The SAI of the previous October displays a stable correlation with stations in the northern mountains of the Douro Basin and the Mediterranean Andalusian Basin (reaching values of around 0.56 in this basin). The NAO and AO of the previous winter were found to be stable predictors, particularly for stations in Mediterranean Andalusian Basin. In this case, the correlation values reach up to 0.7 and 0.6 for NAO and AO, respectively. Although the winter, spring, and summer WeMO appear as a potential predictor, they do not display a similar correlation map. Winter WeMO correlates stably with stations in the Mediterranean Andalusian Basin, whereas spring and summer WeMO present stable correlations with stations in the northern basins (mostly in Miño-Sil, Douro, and upper Ebro). Spring and summer East Atlantic were found to be a stable predictor for stations in Miño-Sil Basin and also for some located in the headwaters of the Douro and Tagus. The EP-NP of the previous spring also shows stable correlations with a remarkable number of stations (74) situated in the northwestern quadrant of the IP. El Niño3.4 and SOI in summer present stable correlation with some stations in northern half of IP. However, it bears noting that the sign of these correlations is the opposite of that found for the previous autumn ENSO indices.

For the winter streamflow, Figure 6 displays the correlation maps for the stable predictors. Although previous winter EMI and WeMO show stable correlation with few stations, they are grouped. A notable number of stations (67) present stable correlations with previous spring WP, particularly in the Douro, Tagus, and Guadalquivir Basins. However, the magnitude of these correlations is weak (0.40 in average). Previous spring EP-NP, summer PNA, and autumn SCAND also show stable but weak correlations (around 0.40 and 0.45 on

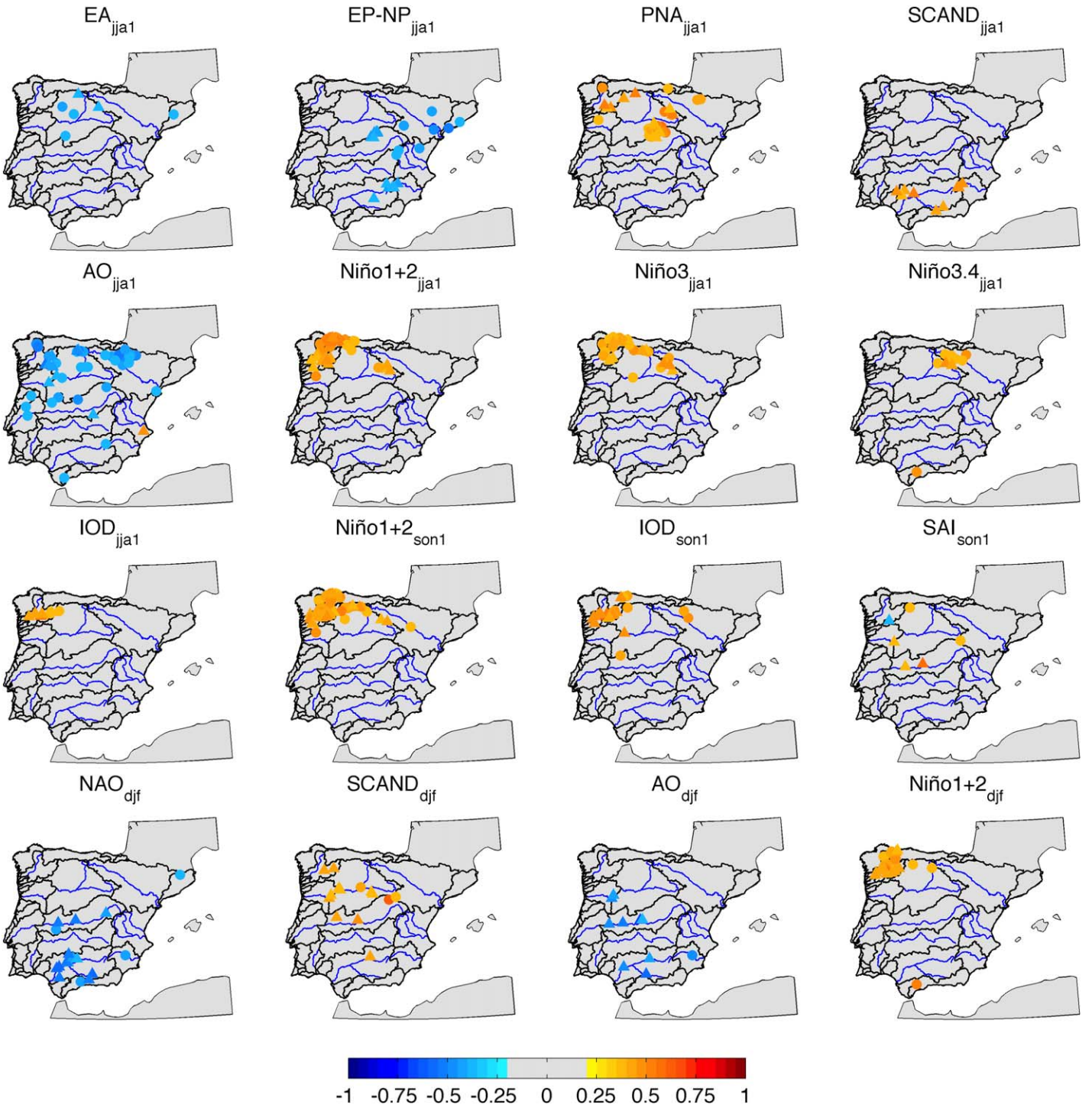

Figure 7. As Figure 5 but for spring (AMJ) streamflow.

average), mainly in the Douro, Tagus, and Ebro for spring EP-NP, the Douro and Tagus for summer PNA and, in case of autumn SCAND, the Miño-Sil, Douro, Tagus, and Ebro Basins. Previous autumn WeMO also presents stable correlations in stations on the Mediterranean slope. Finally, the most remarkable results are found for the SAI of the previous October, which has stable correlations with 238 stations, except with those located near the Cantabrian and Mediterranean slopes. In addition, the average of these correlations is higher (around 0.6) than observed with all the previous indices.

Table 1. Teleconnection Indices Used as Predictors of Autumn, Winter, and Spring Streamflow in Each Forecasting Scenarios

SCENARIOS									Streamflow
4S	3S		2S			1S			
WP_{son1} $Niño3_{son1}$ $Niño4_{son1}$ $Niño3.4_{son1}$ SOI_{son1} SAI_{son1}	WP_{son1} $Niño3_{son1}$ $Niño4_{son1}$ $Niño3.4_{son1}$ SOI_{son1} SAI_{son1}	NAO_{dif} AO_{dif} $Niño4_{dif}$ $WeMO_{dif}$	WP_{son1} $Niño3_{son1}$ $Niño4_{son1}$ $Niño3.4_{son1}$ SOI_{son1} SAI_{son1}	NAO_{djf} AO_{djf} $Niño4_{djf}$ $WeMO_{djf1}$	EA_{mam} WP_{mam} $EP\text{-}NP_{mam}$ $WeMO_{mam}$	WP_{son1} $Niño3_{son1}$ $Niño4_{son1}$ $Niño3.4_{son1}$ SOI_{son1} SAI_{son1}	NAO_{dif} AO_{dif} $Niño4_{dif}$ $WeMO_{dif}$	EA_{mam} WP_{mam} $EP\text{-}NP_{mam}$ $WeMO_{mam}$	EA_{jia} $Niño3.4_{jia}$ SOI_{jia} $WeMO_{jja}$	**OND**
EMI_{djf1} $WeMO_{djf1}$	EMI_{dif1} $WeMO_{dif1}$	WP_{mam1} $EP\text{-}NP_{mam1}$ PNA_{mam1}	EMI_{djf1} $WeMO_{djf1}$	WP_{mam1} $EP\text{-}NP_{mam1}$ PNA_{mam1}	PNA_{jja1}	EMI_{dif1} $WeMO_{dif1}$	WP_{mam1} $EP\text{-}NP_{mam1}$ PNA_{mam1}	PNA_{jja1}	$SCAND_{son1}$ $WeMO_{son1}$ SAI_{son1}	**JFM**
		EA_{jia1} $EP\text{-}NP_{jia1}$ PNA_{jia1} $SCAND_{jia1}$ AO_{jia1} $Niño1{+}2_{jia1}$ $Niño3_{jia1}$ $Niño3.4_{jia1}$ IOD_{jja1}		EA_{jja1} $EP\text{-}NP_{jja1}$ PNA_{jja1} $SCAND_{jja1}$ AO_{jja1} $Niño1{+}2_{jja1}$ $Niño3_{jja1}$ $Niño3.4_{jja1}$ IOD_{jja1}	$Niño1{+}2_{son1}$ IOD_{son1} SAI_{son1}		EA_{jia1} $EP\text{-}NP_{jia1}$ PNA_{jia1} $SCAND_{jia1}$ AO_{jia1} $Niño1{+}2_{jia1}$ $Niño3_{jia1}$ $Niño3.4_{jia1}$ IOD_{jja1}	$Niño1{+}2_{son1}$ IOD_{son1} SAI_{son1}	NAO_{dif} $SCAND_{dif}$ AO_{dif} $Niño1{+}2_{djf}$	**AMJ**

In case of spring streamflow (Figure 7), while no index in the previous spring is identified as a predictor, up to 9 teleconnection indices of the previous summer do. In particular, summer EA correlates stably with stations in the Douro Basin. The summer EP-NP correlates with the stations in the eastern IP, the summer SCAND with stations in the Guadalquivir Basin, and summer PNA appears as a potential predictor of spring streamflow for stations located in the Miño-Sil, Douro, and Tagus Basins. ENSO-related indices in summer (Niño1+2, Niño3, Niño3.4, and IOD) present stable correlations with spring streamflow in stations located in the Miño-Sil, Cantabrian, and Douro Basins as well as with some in the upper Ebro Basin. The presence of ENSO-related indices as a stable predictor extends through the autumn (Niño1+2 and IOD) and winter (Niño1+2). Also, previous October SAI and winter NAO/AO correlate stably with stations in the Douro, Tagus, and Guadalquivir Basins, especially in case of NAO and AO, and winter SCAND correlates stably with stations in the Miño-Sil, Douro, and Tagus Basins. The magnitude of these correlations is, in general, relatively weak (around 0.4 and 0.45), the previous winter NAO being the index presenting the highest correlations (−0.48 in average).

4.2. Forecasting Skill Evaluation

The teleconnection indices used as predictors of autumn, winter, and spring streamflow in each forecasting scenarios are presented in Table 1. Note that for spring streamflow there are no predictors for the 4S scenario (no index in the previous spring was considered to be a stable predictor).

Prior to evaluating the quality of the forecasting results, we briefly noted the way in which the possible problems derived from multicollinearity were addressed. We carefully checked the results from the combined VIF and backward selection iterative procedures, particularly when some of the indices representing the ENSO phenomenon were considered as predictors. As a result, we noted that when several of the indices were selected as predictors, only one of them remained after applying both selection methods.

Concerning the results from the comparison between the observed and forecasted seasonal streamflow, a classification was established according to the values of the verification skill scores:

1. Bad: RHO $<$ 0.34 or RMSESS $<=$ 0 or GSS $<=$ 0

2. Poor: RHO $>=$ 0.34 and RMSESS $>$ 0 and GSS $>$ 0

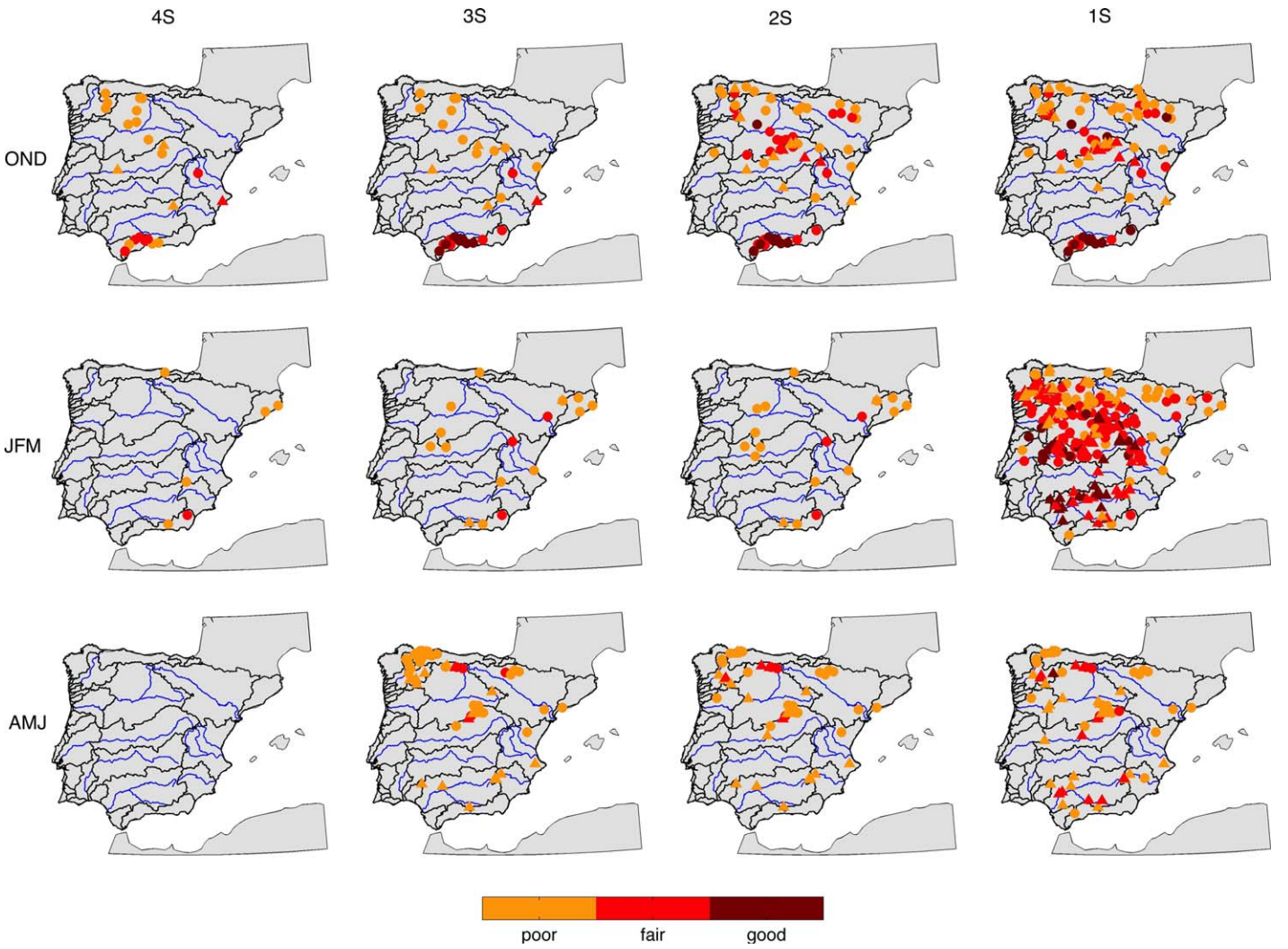

Figure 8. Maps of the forecasting skill classification (poor, fair, or good) according with RHO, RMSESS, and GSS values. Only stations with some forecast skill are displayed. In rows the seasonal streamflow forecasted, and in columns the forecasting scenario.

3. Fair: RHO >= 0.39 and RMSESS > 10 % and GSS > 0.2

4. Good: RHO >= 0.5 and RMSESS > 20 % and GSS > 0.4

Note that the values 0.34 and 0.39 used as thresholds in case of RHO score correspond to the 90% and 95% significance levels in Pearson's correlation coefficient. The thresholds for RMSESS and GSS were selected arbitrarily.

Figure 8 and Table 2 summarize the forecasting results according to this classification. In case of autumn streamflow forecasting, only 24 of the 96 predicted time series present some forecasting skill for the 4S scenario. Some stations located in the Miño-Sil, Douro, and Tagus Basins present poor forecasts, but some located in the Mediterranean Andalusian Basin show fair skill. In the first case (poorly forecasted stations in the Miño-Sil, Douro, and Tagus Basins), the indices related to ENSO phenomena in the previous autumn seem to be responsible and, in the second case, the SAI index of previous October is the predictor used for forecasting autumn streamflow at these stations. Regarding 3S scenario, 30 of the 115 stations where autumn streamflow was forecasted present accurate results. The most noteworthy feature is the improvement in forecasting at stations located in the Mediterranean Andalusian Basin, where most stations present fair and good forecasting results. For these stations, NAO and AO indices of previous winter are the predictors related to this improved forecasting skill. For 2S scenario, forecasting skill somewhat improves (up to 63 stations present some forecasting skill, whereas 127 stations do

Table 2. Number of Stations Belonging to Each of the Classes Defined for Summarizing Forecasting Skill (Bad, Poor, Fair, and Good)[a]

	4S				3S				2S				1S			
	Bad	Poor	Fair	Good	Bad	Poor	Fair	Good	Bad	Poor	Fair	Good	Bad	Poor	Fair	Good
OND	72	17	7	0	85	16	7	7	127	31	24	8	140	43	25	11
JFM	5	5	1	0	73	14	3	0	79	16	3	0	33	70	127	39
AMJ	0	0	0	0	98	46	6	0	125	37	7	0	133	43	15	1

[a]In columns, the four scenarios considered and in rows the seasonal streamflow forecasted (autumn-OND-, winter-JFM-, and spring-AMJ-) streamflow.

not), particularly in the central and northwestern quadrant and in the Ebro Basin. The increase in forecasting skill could be related to the inclusion of spring EP-NP and WeMO patterns. Forecasting skill does not vary notably in 1S scenario (79 stations present some forecasting skill, whereas 140 stations give bad forecasting results).

The winter streamflow, in the 4S scenario is forecasted only in 11 stations, being skillful in 6 of them. In the 3S scenario, when spring WP and EP-NP patterns were added to winter EMI and WeMO as predictors, the winter streamflow is predicted in 90 stations. However, these predictors were considered skillful in only 17 of them (mostly poorly forecasted). In addition, there is no remarkable improvement in the forecasting results when summer PNA was added as predictor for the 2S scenario. However, a substantial increase in forecasting skill is achieved in 1S scenario. In this case, winter streamflow was forecasted at 269 stations, being skillful in 236 of them. In particular, at 166 stations, the forecasting is considered fair or good, with RHO reaching values above 0.6, RMSESS up to 30% and GSS above 0.6 for some cases. The SAI is the predictor responsible for this noteworthy improvement in the forecasting results. The stations that present some forecasting skill are located in most of the IP, with the exception of the Cantabrian range and some areas in the Mediterranean slope.

In case of spring streamflow forecasting, there was no predictor for the 4S scenario. For 3S scenario, up to nine predictors are used (from teleconnection indices in the previous summer). In this case, spring streamflow is predicted in 150 stations, but only in 52 of them with some skill (mostly poor). The stations where some forecasting skill is found are located mainly in the Miño-Sil, mountains surrounding the Douro Basin borders, and Guadalquivir Basin. When predictors corresponding to the previous autumn are added to the forecasting model (2S scenario), there is no improvement in the forecasting results. In fact, the number of stations with skillful forecasted spring streamflow is slightly inferior (probably because the verification scores are low enough to fall below the classification thresholds). In case of the 1S scenario, the use of winter NAO, SCAND, and AO indices improve the forecasting results (up to 58 stations skillfully forecasted), particularly in the southern of IP.

Finally, an example of the forecasting for the seasonal time series (standardized) is shown in Figure 9, displaying the results for one station in each season (OND streamflow in station id = 10020, JFM streamflow in station id = 3144 and AMJ streamflow in station id = 1710, where "id" indicates the identifier of each station). The stations were selected from among the most skillfully forecasted with the consideration of being located in different basins. The values of the verification scores are given in Table 3. In Figure 9a, station id = 10020 is used as an example of autumn streamflow forecasting in the 3S scenario. This station is located in the Mediterranean Andalusian Basin (Figure 9a, left). The predictor used (after backward stepwise selection) was the previous winter NAO. Figure 9a (middle) shows the good agreement between the observed and forecasted autumn streamflow (RHO, RMSESS and GSS are 0.67, 21.1%, and 0.45, respectively). That is also manifested in the Figure 9a (right), where the time series of both observed and forecasted streamflow are plotted along with the upper and lower bounds of the prediction interval at 95% confidence level. In particular, the similarity in the 1970s and 1980s is noteworthy. On the other hand, the variability in the 1990s is not completely reproduced. Figure 9b (left) presents the forecasting results for winter streamflow in station id=3144 in the Tagus Basin for 1S forecasting scenario. In this case, October SAI and spring WP were the two predictors selected in the backward stepwise procedure (the SAI being the most correlated predictor). In this case, verification scores are even higher than in the previous example (RHO, RMSESS, and GSS are 0.72, 29.8%, and 0.66, respectively), as reflected in Figure 9b (middle and right), where the good agreement between observed and forecasted time series is evident. Figure 9c (left) shows an example

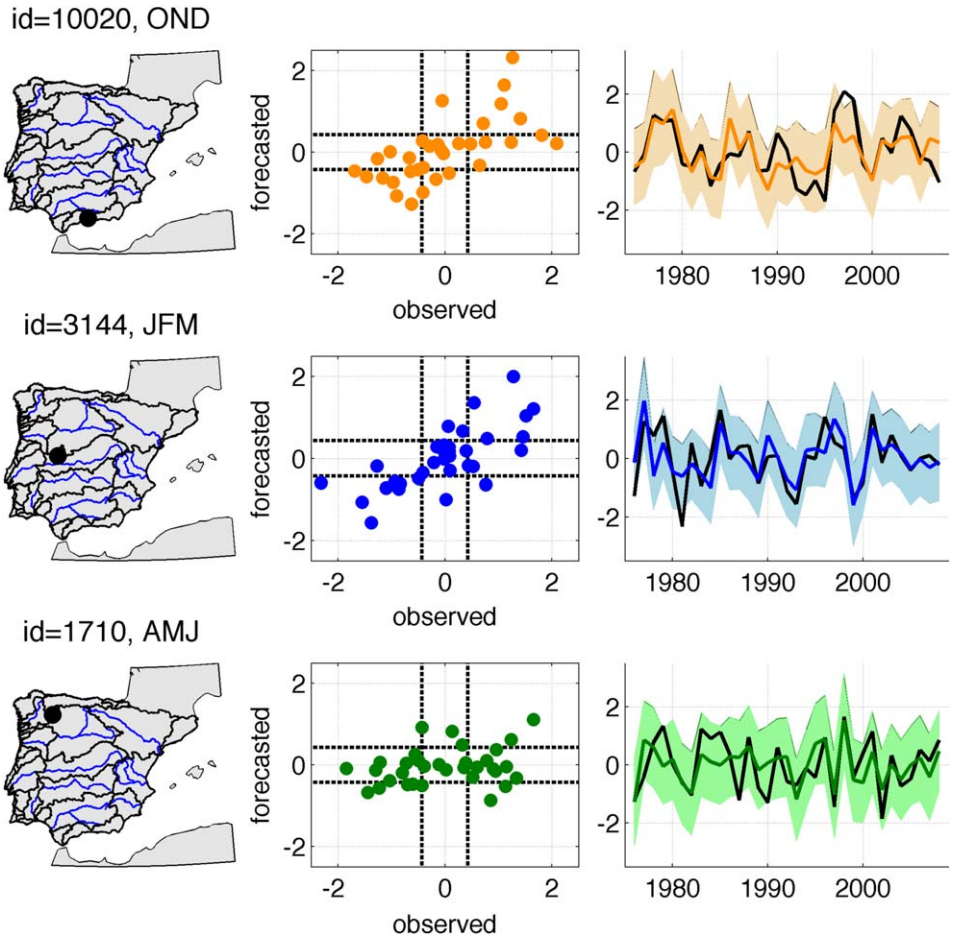

Figure 9. In rows, an example of forecasted seasonal streamflow time series for a gauging station in each season. (a) for autumn streamflow in station id = 10020 (Mediterranean Andalusian Basin), (b) for winter streamflow in station id = 3144 (Tagus Basin), and (c) for spring streamflow in station id = 1710 (Miño-Sil Basin). In the left plots, the location of these stations; in the middle plots, scatter plots between the observed and forecasted seasonal streamflow in each station (black-dashed line indicates the 33rd and 66th percentiles); and in the right plots, the observed (black line) and forecasted (colored lines) streamflow time series in each forecasting scenario. Shaded bands indicate the upper and lower bounds of the prediction interval at 95% confidence level.

of spring streamflow forecasting in scenario 1S. The station selected is located in the Miño-Sil Basin. The verification scores reach values up to 0.63, 20.6%, and 0.43 for RHO, RMSESS, and GSS, respectively. The IOD of the previous autumn and the SCAND of previous winter constitute the predictors selected after the combination of VIF and backward stepwise selection. From the observed and forecasted time series displayed in Figure 9c (right), the forecasting skill improves after the 1990s, whereas the variability of the forecasted time series during the 1980s is significantly lower than the observed streamflow.

5. Discussion

In this paper, we have identified stable correlations between seasonal teleconnection indices and lagging seasonal streamflow in the IP. Based on these stable correlations, teleconnection indices leading seasonal streamflow have been evaluated as potential predictors. However, understanding the physical mechanisms

Table 3. Values of the Verification Scores (RHO, RMSESS, and GSS) for the Three Stations Selected as Examples in Figure 9

Season	Station Id	Basin	Scenario	RHO	RMSESS	GSS	CLASS
OND	10020	Mediterranean Andalusian	3S	0.67	21.1 %	0.45	Good
JFM	3144	Tagus	1S	0.72	29.8 %	0.66	Good
AMJ	1710	Miño-Sil	1S	0.63	20.6 %	0.43	Good

responsible for these relationships requires additional analysis. The connection between teleconnection indices leading seasonal streamflow in some months or seasons in the IP might be explained through changes in slowly varying boundary conditions, such as SST or ice-sea extension in the Arctic or the snow cover in high-latitude land masses. Moreover, the individual features of each basin play an important role in the lag response to the teleconnection indices, in particular on shorter time scales (one season) responses. To evaluate this, a hydrological model would be needed for each individual basin. With the large number of teleconnection indices and seasonal streamflow analyzed, a detailed description of the physical basis of these relationships becomes a substantial amount of work and is beyond the scope of this study. Nonetheless, based on the literature, we postulate on which of the physical links might explain the most noteworthy relationships.

5.1. Teleconnection Indices as Predictors of Autumn Streamflow

A noteworthy result found in this work is the strong correlation (above 0.6 in absolute values) found between October SAI and winter NAO and AO with following autumn streamflow in the Mediterranean Andalusian Basin (Figure 5). As was introduced in section 2, the SAI is considered a useful index for predicting winter conditions in the North Atlantic, in particular winter AO and NAO, which are major drivers of winter precipitation in the western IP. However, the relationship between NAO and precipitation in the Mediterranean slope of the IP is weak. We examined the correlation between winter (December–February) NAO and winter (January–March) streamflow in the Mediterranean Andalusian Basin, which is not significant in most of stations (not shown). A possible link between winter NAO/AO and October SAI with following OND streamflow in the Mediterranean Andalusian Basin could be through later spring and summer snowmelt contribution. This basin is located between the Mediterranean Sea and the Betics System, a high-mountain ridge (with the highest peaks of the IP, i.e., over 3000 m high), which accumulates large amounts of snow during winter (it acts as a natural barrier for fronts coming from Atlantic Ocean in winter). Thus, the snowmelt during late spring and summer months could contribute to an increase in runoff during the summer months, and this effect could remain until the next autumn. To corroborate this hypothesis, we evaluated the correlation between summer (June–August) and autumn (October–December) streamflow in this basin. As a result, only 3 of the 15 stations presented a significant correlation, so we discarded this hypothesis. Consequently, the explanation for the connection between these indices and autumn streamflow in the Mediterranean Andalusian Basin needs additional analyses. A possible physical explanation of this relationship might be in the line of the results found by *Báez et al*. [2013]. These authors postulated a relationship between winter NAO and AO conditions and following summer SST in the Alboran Sea (a part of the Mediterranean Sea close to the Mediterranean Andalusian Basin), through the accumulated snow in Sierra Nevada, which increases the input of continental freshwater in the Alboran Sea during summer, maintaining the mixed layer at a greater depth and increasing the SST. With this hypothesis borne in mind, warmer than average SSTs in the Mediterranean could lead to enhanced local evaporation, and hence to increased lower-tropospheric humidity. This additional moisture is likely to be advected from the western Mediterranean to the southern IP during late summer and autumn and, together with the rugged terrain, promote greater rainfall over this area. Note that an atmospheric configuration at sea level providing advection from the Mediterranean together with a cutoff low in the upper levels, have been associated with intense rainfall events over southeastern Spain during autumn [*Hidalgo-Muñoz et al*., 2011].

The WeMO index has also been identified as a stable predictor for seasonal streamflow (with different lags). The WeMO index has been associated with extreme precipitation events over the Mediterranean slope of the IP [*Martin-Vide et al*., 2008; *Hidalgo-Muñoz et al*., 2011], particularly during autumn and early winter. We calculated the correlation between WeMO and streamflow in autumn (not shown), finding stable positive correlations in the Cantabrian range and negative in the Mediterranean slope. The positive phase of WeMO resembles a low/high pressure centre in Padua/Gibraltar. This configuration favors the entrance of humid winds from the Atlantic Ocean/Cantabrian Sea that bring about precipitation on the northern slope of the Cantabrian ranges. Correspondingly, positive correlations with the Cantabrian Basin were found when September–November WeMO was correlated with October–December streamflow (not shown). Similarly, Figure 5 displays a positive correlation in the Upper Ebro (near the Cantabrian coast) between summer WeMO and following autumn streamflow. Thus, it seems that the origin of this teleconnection is likely due to a lagging response of streamflow. However, the

teleconnection between previous winter and spring WeMO with autumn streamflow is not well understood as a lagging response to the coetaneous relationship between WeMO and precipitation in the IP. This sea-level pressure configuration related to WeMO phases could be a regional reflection of a larger-scale phenomenon. Nevertheless, further analyses are needed.

In relation with the lagging influence of teleconnection indices located in the Pacific, ENSO indices have also been found to be stably correlated with autumn (Figure 5), especially with stations located in the northwestern quadrant of the IP. Numerous studies have demonstrated statistical associations between ENSO and precipitation in the Mediterranean Basin. In case of the IP, precipitation has been shown to increase during late summer, autumn, and early winter when El Niño conditions are present in the Pacific [*Rodó et al*., 1997; *Mariotti et al*., 2002; *Park*, 2004; *Pozo-Vázquez et al*., 2005; *Vicente-Serrano and López-Moreno*, 2005; *Sordo et al*., 2008]. In agreement with this, positive correlations were found between summer ENSO indices (which represent the beginning of the phenomenon) and following OND streamflow (Figure 5). Also, we conducted a correlation analysis between September and November ENSO indices and October and December streamflow, finding an increase in the number of stations with positive correlations. Hence, the link between autumn and early winter ENSO with autumn and early winter streamflow in the IP begins in summer, with the beginning of the phenomenon. Also notable was the contrary sign observed between previous autumn and winter ENSO indices with autumn streamflow of the following year with respect to the correlation between summer and autumn ENSO indices and autumn streamflow of the same year. This change in the sign of the correlation, also observed by *Córdoba-Machado et al*. [2015] in a study of the relationship between Pacific SST and precipitation in Colombia, could be related to a 2 year periodicity observed in El Niño [*Yu and Kim*, 2010]. Regarding the dynamical mechanisms relating ENSO state and precipitation anomalies in the southwestern Europe [*Giannini et al*., 2001; *Shaman and Tziperman*, 2011; *Shaman*, 1999, among others], *Park* [2004] proposed that an eastward Rossby wave train emanating from the Pacific during late summer and autumn might be responsible for the changes over the Mediterranean. More recently, *Shaman and Tziperman* [2011] indicated that precipitation anomalies are associated with changes in large-scale atmospheric fields to the west of the IP that alter low-level westerly winds and onshore moisture advection from the Atlantic.

5.2. Teleconnection Indices as Predictor of Winter Streamflow

One of the most remarkable results is the acceptable winter streamflow prediction in a high number of gauging stations found when the SAI of the previous October is used as the predictor. These results agree with those of *Brands et al*. [2012, 2014], who found reasonable forecasting skill for winter precipitation over the central and western IP when using the SAI as the predictor. The role that Eurasian snow cover plays in the winter NH climate has attracted greater attention in the last two decades [*Cohen and Saito*, 2003; *Gong et al*., 2003; *Cohen and Flecher*, 2007; *Cohen et al*., 2007, among others]. The links between observed snow cover and NH wintertime circulation were also reproduced by model simulations [*Orsolini and Kvamstø*, 2009]. *Cohen and Entekhabi* [1999] showed that the Eurasian snow cover in early fall is significantly correlated with the following winter Arctic Oscillation (AO). These authors hypothesize that a possible dynamical mechanism linking Eurasian snow cover anomalies and North Atlantic climate variability involves the strength and position of the Siberian High. However, the stationary relationship of Siberian snow-cover extent in the fall and following winter Arctic Oscillation has recently been questioned [*Peings et al*., 2013], indicating that it could be modulated by the Quasi-Biennal Oscillation in the equatorial stratosphere. Thus, the SAI-AO relationship should be taken in careful consideration and examined when more data are available, especially if it is to be used for forecasting purposes.

5.3. Teleconnection Indices as Predictors of Spring Streamflow

Another notable result concerns the stable correlations (negative) identified between summer Arctic Oscillation and seasonal streamflow in following spring (Figure 7), particularly in western or northwestern IP. One possible physical mechanism responsible for this lag relationship could be the associated with summer Arctic Sea ice extension. *Matsumura et al*. [2014] evaluated the influence of spring Eurasian snow cover on summer Arctic atmospheric circulation and the possible linkage with the increased Arctic sea-ice loss. Specifically, they indicate that the reduced albedo due to earlier spring snowmelt over Eurasia leads to a warmer land surface, which amplifies stationary Rossby waves, decelerating the subpolar jet. As a consequence of the rising motion enhanced over land, compensating subsidence and adiabatic

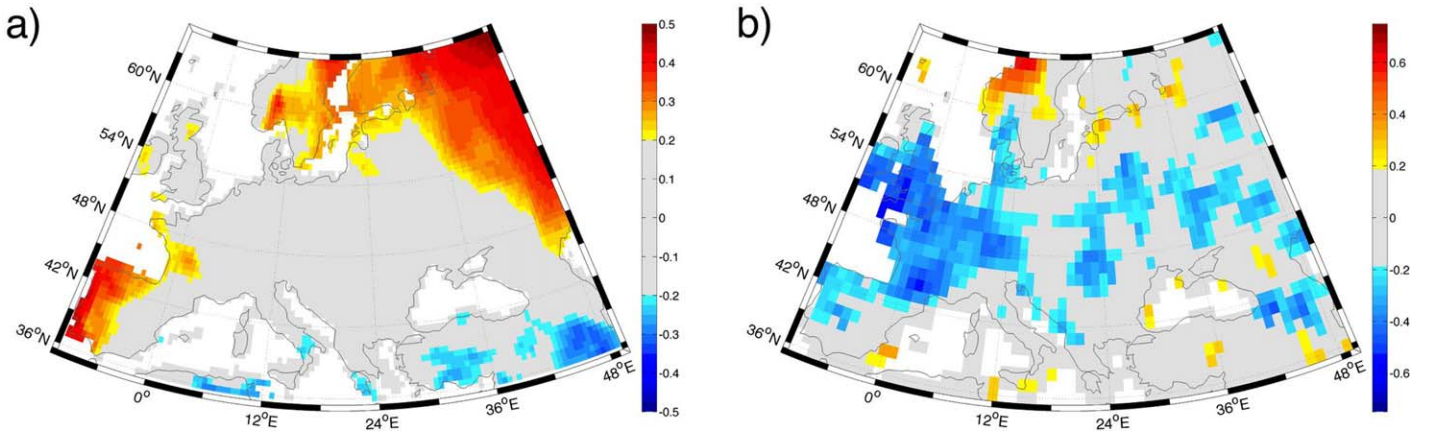

Figure 10. Correlation of summer AO with spring (March to May) (a) temperature and (b) precipitation. Temperature data at 0.5° of spatial resolution were obtained from CRU TS v.3.1 data set. Precipitation data at 1° of spatial resolution where obtained from GPCC Precipitation data set.

heating occur in the Arctic troposphere, forming a negative Northern Annular Mode (NAM). Note that AO and NAM resemble similar height anomalies pattern. The recent trends toward a negative phase of NAM during summer have been linked to the accelerating trend of sea-ice extension retreat in the Arctic during summer [*Ogi and Yamazaki*, 2010]. In addition, the effects of Arctic sea-ice reduction in summer in the midlatitudes weather in the following winter have received special attention in recent years (two noteworthy reviews have been recently published by *Cohen et al*. [2014] and *Vihma* [2014]). In *Cohen et al*. [2014], the authors indicate three possible dynamical pathways through which Arctic amplification may influence midlatitude weather: changes in storm tracks in the North Atlantic sector, in the characteristic jet stream and in the planetary wave configurations. Some of the studies reviewed in *Vihma* [2014], such as the one made by *Francis et al*. [2009] and *Overland and Wang* [2010], suggest that summer sea ice declining in the Arctic causes a deepening of the atmospheric boundary layer, a warming and destabilization of the lower troposphere, and a decreasing of the poleward gradient in the thickness of the atmospheric layer between 500 and 1000 hPa pressure levels, which weakens the polar jet stream. This configuration is similar to a negative phase of Arctic Oscillation. In addition, *Outten and Esau* [2012], on the basis of ERA-Interim reanalysis, identified cooling trends of wintertime near-surface air temperature along a band that extends across midlatitude Eurasia. By their interpretation, the weakened north-south temperature gradient has decreased wintertime westerly winds over midlatitude Eurasia, resulting in lower temperatures. The cooling in northern Eurasia resulting from less sea ice extent in the Arctic in September is also supported by *Rinke et al*. [2013] and *Peings and Magnusdottir* [2013] using model experiments. With these findings in mind, we postulate that this cooling in winter combined with more precipitation could result in an increased snowfall during winter. Consequently, an increase in spring streamflow could be expected by snowmelt contribution. We made a correlation analysis between summer AO and winter and spring temperature (using the CRUTS3.1 temperature dataset, with 0.5° degree of spatial resolution, *Harris et al*. [2014]) and precipitation (using GPCC precipitation dataset, with 1° degree of spatial resolution, *Schneider et al*. [2013]) over Europe. We found significant positive correlation (not shown) with winter temperature over Finland and western Russia. Also some areas in the IP proved positive but with no significant correlations. In the case of spring temperatures (Figure 10a), the above positively correlated area in western Russia increases in extension, and also appears a positive significant correlation in the western half of the IP but a negative correlation with precipitation (Figure 10b). This positive/negative correlation with spring temperature/precipitation over the IP means that negative AO anomalies (or NAM) in summer is linked with below-normal temperature in the western IP in spring (late winter and early spring) and with positive precipitation anomalies and perhaps increased snowfall in mountain ranges because of the lower temperatures. This could explain an above-normal streamflow during spring as a consequence of both higher precipitation and snowmelt contribution. However, uncertainties remain concerning these dynamical pathways [*Cohen et al*., 2014]. For example, although observational analysis has shown links between summer sea-ice loss in the Arctic and winter NAO/AO, modeling simulations do not. Also, there are other factors, besides the near-surface

meridional temperature gradient, influencing the zonal jet that should be considered. In addition, more statistically robust results regarding the influence of alteration in planetary waves over Eurasia are needed.

The correlation found between winter NAO and SCAND with streamflow the following spring (Figure 7) might be associated with the lagging response in each basin and the contribution of snowmelt that accumulated during winter in high-mountain systems, as NAO and SCAND are major teleconnection indices driving winter precipitation in the western IP [*Rodriguez-Puebla et al*., 2001].

In relation with the lagging influence of teleconnection indices located in the Pacific, ENSO indices have also been found to be stably correlated with spring (Figure 7) streamflow, especially with stations located in the northwestern quadrant of the IP. *Rodó et al*. [1997] and *Knippertz et al*. [2003] found an association between boreal winter ENSO conditions and spring precipitation over Spain and southwestern Europe, respectively. Furthermore, *Mariotti et al*. [2002] found that precipitation in the Mediterranean area in late winter and spring is suppressed during an El Niño event. However, *Lorenzo et al*. [2010] concluded that the negative phase of ENSO, "La Niña," almost always announces dry springs in northwestern IP, whereas the positive phase of ENSO, "El Niño," does not anticipate the appearance of wet springs. In line with these results (negative ENSO associated with negative precipitation), we found stable positive correlations in spring streamflow in the northeastern basins (Figure 7) with ENSO related indices (such as Niño1+2, Niño3, Niño3.4, IOD, PNA) in summer and autumn. *Bulic and Kucharski* [2012] indicated that Rossby wave propagation mechanism is too fast to be responsible for such a delayed impact of winter SST anomalies in tropical Pacific on spring precipitation over the North Atlantic/European. Instead they suggest that a chain of air-sea interaction may explain the delayed response, establishing the link between the tropical Pacific and extratropical SST anomalies via the so-called "atmospheric bridge." Other teleconnection patterns related to atmospheric variability in the Pacific have also been identified as a stable predictor, such as summer PNA (for following winter and spring streamflow), spring EP-NP (for following autumn), and spring WP (for following autumn and winter). Studies linking these teleconnection patterns with precipitation or streamflow in southwestern Europe are still scarce. One explanation relating these atmospheric patterns with following autumn to spring is that they reflect changes in tropical Pacific SST or the extent of sea ice in the Arctic. For example, in the discussion in *Pozo-Vázquez et al*. [2005], the PNA is proposed as one of the links between tropical forcing and extratropical circulation response in the North Atlantic area, triggering a standing wave train that propagates downstream to the North Atlantic area. In the case of WP, recent works, such as in *Linkin and Nigam* [2008], have related the WP with the sea-ice extent in marginal zones in the Arctic, establishing relationships with PNA and ENSO in the Pacific. However, how this pattern influences streamflow in late autumn and winter is still a matter of study.

6. Conclusions

This paper provides a systematic evaluation of potential predictability of teleconnection indices leading up to 1 year seasonal (autumn, winter, and spring) streamflow of IP Rivers. To give a complete spatial perspective of the IP, we used a database of 382 gauging stations covering the main basins of the IP. This database passed a quality control to ensure they were not strongly affected by inhomogeneities, particularly of the type caused by alteration of the natural streamflow regime as a consequence of water-resource management in upstream reservoirs. The forecasting methodology, based on multiple linear-regression models, was developed for four forecasting scenarios, related to the number of seasons prior to which the forecasting is made, from 1 year until one season in advance, updating and improving the predictions seasonally. This approach becomes a useful tool for decision making related to water management, since predictions are given with different seasons in advance. As predictors, from an original set of up to 20 teleconnection indices representing most of the large-scale atmospheric and oceanic variability, those with stable correlations with a large enough amount of stations were used. The question of multicollinearity among predictors was addressed by combining two iterative methods in the regression analysis: variance inflation fraction and backward stepwise selection. According to the results described in section 4, the following conclusions can be summarized:

1. Regarding autumn streamflow forecasting, reasonable good predictions (with RHO $>$ 0.5, RMSESS $>$ 20% and GSS $>$ 0.4) are found for stations located in the Mediterranean Andalusian Basin, particularly from 3S scenario (i.e., considering the information provided by seasonal teleconnection indices from previous autumn and winter). In these cases, the SAI measured in October of the previous year, and the previous

winter NAO and AO indices constitute the predictors used. Moderately accurate predictions (RHO > 0.44, RMSESS > 10% and GSS > 0.2) were also found in the 3S and 2S scenario for stations located the northern basins of IP (Miño-Sil, Douro, Ebro, and Tagus Basins), ENSO indices in the previous autumn, together with spring EP-NP and WeMO indices being the most widely used predictors.

2. For winter streamflow forecasts, in scenarios 4S, 3S, and 2S, forecasting skill was found only in stations located in the Mediterranean sector, although most of them presented poor forecasting skill. On the other hand, a significant number of stations (168) presented moderate or good predictions (with RHO > 0.44, RMSESS > 10% and GSS > 0.2) for the 1S scenario, especially in basins located in the central and western IP. The SAI was identified as the main predictor for winter streamflow, in both the number of stations significantly correlated and the highest correlation values. From this result, teleconnection indices are not able to predict winter streamflow more than 2 months in advance, and only when the October SAI is added, skillful predictions are made. These results agree with those of *Brands et al*. [2012, 2014], who forecasted winter precipitation with reasonable skill over the central and western IP by using the SAI as the predictor. In addition to this, SAI is a very helpful predictor not only for following winter precipitation and streamflow but also for following autumn streamflow in Mediterranean Andalusian Basin. Bearing in mind that the temporal coverage of the "daily" version of SAI (which presents higher correlations with JFM streamflow than the "weekly" version) is still short, we conclude that the larger time series of SAI available, the more skillful winter streamflow forecasting.
3. Spring was the season with the poorest results in streamflow forecasting (only 17 stations showed moderate or good predictions in the most favorable scenario, 1S). Stable positive correlations were found with indices related to atmospheric or oceanic variability in the Pacific, such as Niño1+2, Niño3, Niño3.4, IOD, PNA, or EP-NP in summer for stations in the northwest. Also, summer AO was found to be a stable predictor of stations in the northern half of the IP. In the case of stations located in central and southern basins of the IP, the previous winter SCAND and NAO are the teleconnection indices best correlated with them.

In summary, this study provides valuable information regarding the impact of climate variability (represented by teleconnection indices) on seasonal streamflow in the Iberian Peninsula, offering a helpful tool for the sustainable management of water resources. The use of an approach based on seasonally updated predictions allows the option of developing water-management policies some seasons in advance and with the possibility of modifying or adjusting these strategies as the predictions are updated. Having skillful forecasting with several months in advance provides helpful information for water-management strategies. However, there are some limitations in this work to be overcome in future studies, such as the predefined character of teleconnection indices, which could be solved by exploring the relationship between climate variables (sea surface temperature or atmospheric pressure) with seasonal streamflow. Furthermore, some results have to be considered with certain degree of caution, especially when the physical link with the predictors used is not fully understood. In addition, the evaluation of a large subset of teleconnection indices supplies useful information of lag relationships between large-scale atmospheric and oceanic variability and seasonal streamflow. Moreover, the examination of a nonlinear relationship between teleconnection indices and seasonal streamflow, such as the study of the streamflow response to ENSO, PDO, or AMO phases, could improve forecasting results, although this requires longer time series.

Appendix A: Data Quality Control

The Pettitt test was selected among the tests proposed by *Kundzewicz and Robson* [2004] to analyze the possible existence of abrupt changes in the seasonal streamflow time series. An advantage of this test is that it is nonparametric, so it does not assume that the data fit any probability distribution. Also, this test is more sensible to detect break points in the middle of the series and it is considered robust in terms of changes in the shape of the distribution of the data. Note that the Pettitt test has been applied to the "extended" seasonal streamflow time series of the 504 stations selected. The term "extended" means that all available records were considered, not only those covering the period from October of 1975 to November of 2008. The reason behind this is that the effects of river regulation could appear before 1975, and the time series for the period 1975–2008 could not reflect the natural behavior of the river flow.

To evaluate whether an abrupt change found for Pettitt test could be related to a change in the natural behavior, we used an additional indicator. This indicator, called the "Common Area Index" (CAI), was defined as the percentage of common area between the curves of the annual cycles calculated using data from before and after the change point. In summary, we applied the Pettitt test to the seasonal (autumn, winter, spring, and summer) time series. For 375 of the 504 stations, this test found a break point in at least one seasonal time series (mainly in spring and summer, and in stations located in the Mediterranean slope as well as in the headwaters of main rivers). We calculated for each station as many CAI as different years of the breaking point. If the smaller value of all CAI calculated for each station was above 50%, the streamflow time series at this station is considered homogeneous, since the regime is not strongly affected after the break. If one of these CAI falls below 50%, the time series at this station is considered not to be homogeneous and is eliminated from subsequent analyses.

Acknowledgments

Streamflow data sets were kindly provided by the Centro de Estudios Hidrográficos (CEDEX, *http://hercules.cedex.es/anuarioaforos/default.asp*), the Agència Catalana de l'Aigua (ACA, *http://aca-web.gencat.cat/aca/appmanager/aca/aca/*), the Agencia Andaluza del Agua (AAA, http://www.agenciamedioambienteyagua.es/), and the Sistema Nacional de Informaçao de Recursos Hídricos (SNIRH, http://snirh.pt/) of Portugal. Teleconnection indices were downloaded from Climate Prediction Centre (CPC, www.cpc.noaa.gov), the Japan Agency for Marine-Earth Science and Technology (www.jamstec.go.jp/), the NPGO website (http://www.o3d.org/npgo/), and the WeMO website (http://www.ub.edu/gc/English/wemo.htm). Justin Jones kindly provided the time series of Snow Advanced Index in personal communication. The authors thanks AEMET and UC by the data provided for this work (Spain02 gridded precipitation data set). The Spanish Ministry of Science and Innovation, with additional support from the European Community Funds (FEDER), projects CGL2010-21188/CLI and CGL2013-48539-R, and the Regional Government of Andalusia, project P11-RNM-7941, had financed this study.

References

AEMET (2011), *Atlas Climático Ibérico*, 80 pp., Minist. de Medio Ambiente y Medio Rural y Marino, Agencia Estatal de Meteorol., Madrid, España.

Aziz, O. A., G. A. Tootle, C. Moser, T. C. Piechota, and K. W. Lamb (2011), Upper Colorado River and Great Basin stream flow and snowpack forecasting using Pacific oceanic–atmospheric variability, *J. Hydrol.*, *410*, 167–177.

Aziz Oubeidillah, A., G. Tootle, and S.-R. Anderson (2012), Atlantic Ocean sea-surface temperatures and regional streamflow variability in the Adour-Garonne basin, France, *Hydrol. Sci. J.*, *57*(3), 496–506.

Báez, J. C., L. Gimeno, M. Gómez-Gesteira, F. Ferri-Yáñez, and R. Real (2013), Combined effects of the North Atlantic oscillation and the Arctic oscillation on sea surface temperature in the Alborán Sea, *PLoS ONE*, *8*(4), e62201, doi:10.1371/journal.pone.0062201.

Bardin, M. Y., and E. N. Voskresenskaya (2007), Pacific decadal oscillation and European climatic anomalies, *J. Phys. Oceanogr.*, *17*(4), 200–208.

Barnston, A. G., and R. E. Livezey (1987), Classification, seasonality and persistence of low-frequency atmospheric circulation patterns, *Mon. Weather Rev.*, *115*(6), 1083–1126.

Bojariu, R., and L. Gimeno (2003), The role of snow cover fluctuations in multiannual NAO persistence, *Geophys. Res. Lett.*, *30*(4), 1156, doi: 10.1029/2002GL015651.

Brands, S., R. Manzanas, J. M. Gutiérrez, and J. Cohen (2012), Seasonal predictability of wintertime precipitation in Europe using the snow advance index, *J. Clim.*, *25*(12), 4023–4028.

Brands, S., S. Herrera, and J. M. Gutiérrez (2014), Is Eurasian snow cover in October a reliable statistical predictor for the wintertime climate on the Iberian Peninsula?, *Int. J. Climatol.*, *34*(5), 1615–1627.

Bretherton, C. S., M. Widmann, V. P. Dymnikov, J. M. Wallace, and I. Bladé (1999), The effective number of spatial degrees of freedom of a time-varying field, *J. Clim.*, *12*(7), 1990–2009.

Bulic, I., and F. Kucharski (2012), Delayed ENSO impact on spring precipitation over North/Atlantic European region, *Clim. Dyn.*, *38*(11–12), 2593–2612.

Casanueva, A., C. Rodríguez-Puebla, M. D. Frías, and N. González-Reviriego (2014), Variability of extreme precipitation over Europe and its relationships with teleconnection patterns, *Hydrol. Earth Syst. Sci.*, *18*(2), 709–725.

Chandimala, J., and L. Zubair (2007), Predictability of stream flow and rainfall based on ENSO for water resources management in Sri Lanka, *J. Hydrol.*, *335*, 303–312.

Chiew, F. H. S., and T. A. McMahon (2002), Global ENSO-streamflow teleconnection, streamflow forecasting and interannual variability, *Hydrolog. Sci. J.*, *47*(3), 505–522.

Chiew, F. H. S., S. L. Zhou, and T. A. McMahon (2003), Use of seasonal streamflow forecasts in water resources management, *J. Hydrol.*, *270*(1–2), 135–144.

Cohen, J., and D. Entekhabi (1999), Eurasian snow cover variability and northern hemisphere climate predictability, *Geophys. Res. Lett.*, *26*(3), 345–348.

Cohen, J., and C. Fletcher (2007), Improved skill of Northern hemisphere winter surface temperature predictions based on land-atmosphere fall anomalies, *J. Clim.*, *20*(16), 4118–4132.

Cohen, J., and J. Jones (2011), A new index for more accurate winter predictions, *Geophys. Res. Lett.*, *38*, L21701, doi:10.1029/2011GL049626.

Cohen, J., M. Barlow, P. J. Kushner, and K. Saito (2007), Stratosphere-troposphere coupling and links with Eurasian land surface variability, *J. Clim.*, *20*(21), 5335–5343.

Cohen, J., et al. (2014), Recent Arctic amplification and extreme mid-latitude weather, *Nat. Geosci.*, *7*(9), 627–637, doi:10.1038/ngeo2234.

Cohen, J. L., and K. Saito (2003), Eurasian snow cover, more skillful in predicting U.S. winter climate than the NAO/AO?, *Geophys. Res. Lett.*, *30*(23), 2190, doi:10.1029/2003GL018053.

Córdoba-Machado, S., R. Palomino-Lemus, S. Gámiz-Fortis, Y. Castro-Díez, and M. J. Esteban-Parra (2015), Influence of tropical Pacific SST on seasonal precipitation in Colombia: Prediction using El Niño and El Niño Modoki, *Clim. Dyn.*, *44*, 1293–1310, doi:10.1007/s00382-014-2232-3.

de Castro, M., N. Lorenzo, J. J. Taboada, M. Sarmiento, I. Álvarez, and M. Gomez-Gesteira (2006), Influence of teleconnection patterns on precipitation variability and on river flow regimes in the Miño River basin (NW Iberian Peninsula), *Clim. Res.*, *32*(1), 63–73.

Dettinger, M. D., and H. F. Diaz (2000), Global characteristics of stream flow seasonality and variability, *J. Hydrometeorol.*, *1*, 289–310.

Di Lorenzo, E., et al. (2008), North Pacific gyre oscillation links ocean climate and ecosystem change, *Geophys. Res. Lett.*, *35*, L08607, doi: 10.1029/2007GL032838.

Esteban-Parra, M. J., F. S. Rodrigo, and Y. Castro-Díez (1998), Spatial and temporal patterns of precipitation in Spain for the period 1880–1992, *Int. J. Climatol.*, *18*(14), 1557–1574.

Francis, J. A., W. Chan, D. J. Leathers, J. R. Miller, and D. E. Veron (2009), Winter Northern hemisphere weather patterns remember summer Arctic sea-ice extent, *Geophys. Res. Lett.*, *36*, L07503, doi:10.1029/2009GL037274.

Frauen, C., and D. Dommenget (2012), Influences of the tropical Indian and Atlantic Oceans on the predictability of ENSO, *Geophys. Res. Lett.*, *39*, L02706, doi:10.1029/2011GL050520.

Gámiz-Fortis, S., D. Pozo-Vázquez, R. M. Trigo, and Y. Castro-Díez (2008a), Quantifying the predictability of winter river flow in Iberia. Part I: Interannual predictability, *J. Clim.*, *21*, 2484–2502, doi:10.1175/2007JCLI1774.1.
Gámiz-Fortis, S., D. Pozo-Vázquez, R. M. Trigo, and Y. Castro-Díez (2008b), Quantifying the predictability of winter river flow in Iberia. Part II: Seasonal predictability, *J. Clim.*, *21*, 2503–2518, doi:10.1175/2007JCLI1775.1.
Gámiz-Fortis, S. R., M. J. Esteban-Parra, R. M. Trigo, and Y. Castro-Díez (2010), Potential predictability of an Iberian river flow based on its relationship with previous winter global SST, *J. Hydrol.*, *385*(1–4), 143–149.
Gámiz-Fortis, S. R., J. M. Hidalgo-Muñoz, D. Argüeso, M. J. Esteban-Parra, and Y. Castro-Díez (2011), Spatio-temporal variability in Ebro river basin (NE Spain): Global SST as potential source of predictability on decadal time scales, *J. Hydrol.*, *409*(3–4), 759–775.
García-Herrera, R., J. Díaz, R. M. Trigo, and E. Hernández (2005), Extreme summer temperatures in Iberia: Health impacts and associated synoptic conditions, *Ann. Geophys.*, *23*(2), 239–251.
García-Serrano, J., B. Rodríguez-Fonseca, I. Bladé, P. Zurita-Gotor, and A. de la Cámara (2011), Rotational atmospheric circulation during North Atlantic-European winter: The influence of ENSO, *Clim. Dyn.*, *37*(9–10), 1727–1743.
Giannini, A., M. A. Cane, and Y. Kushnir (2001), Interdecadal Changes in the ENSO Teleconnection to the Caribbean region and the North Atlantic oscillation*, *J. Clim.*, *14*(13), 2867–2879.
Gong, G., D. Entekhabi, and J. Cohen (2003), Relative impacts of Siberian and North American snow anomalies on the winter Arctic oscillation, *Geophys. Res. Lett.*, *30*(16), 1848, doi:10.1029/2003GL017749.
González-Rouco, J. F., H. Heyen, E. Zorita, and F. Valero (2000), Agreement between observed rainfall trends and climate change simulations in the Southwest of Europe, *J. Clim.*, *13*(17), 3057–3065.
Gutiérrez, F., and J. A. Dracup (2001), An analysis of the feasibility of long-range streamflow forecasting for Colombia using El Niño-Southern Oscillation indicators, *J. Hydrol.*, *246*(1), 181–196.
Hair, J. F., Jr., R. E. Anderson, R. L. Tatham, and W. C. Black (1995), *Multivariate Data Analysis*, pp. 200–206, Macmillan, N. Y.
Harris, I., P. D. Jones, T. J. Osborn, and D. H. Lister (2014), Updated high-resolution grids of monthly climatic observations: The CRU TS3.10 Dataset, *Int. J. Climatol.*, *34*, 623–642, doi:10.1002/joc.3711.
Hernández-Martínez, M., J. M. Hidalgo-Muñoz, S. R. Gámiz-Fortis, Y. Castro-Díez, and M. J. Esteban-Parra (2014), Temporal variability and potential predictability of the streamflow regimes in the North-Eastern Iberian Peninsula, *River Res. Appl.*, doi:10.1002/rra.2825.
Herrera, S., Gutiérrez, J. M., Ancell, R., Pons, M. R., Frías, M. D. and Fernández, J. (2012), Development and analysis of a 50-year high-resolution daily gridded precipitation dataset over Spain (Spain02). *Int. J. Climatol.*, *32*, *74–85*, doi:10.1002/joc.2256.
Hidalgo-Muñoz, J. M., D. Argüeso, S. R. Gámiz-Fortis, M. J. Esteban-Parra, and Y. Castro-Díez (2011), Trends of extreme precipitation and associated synoptic patterns over the southern Iberian Peninsula, *J. Hydrol.*, *409*(1–2), 497–511.
Hurrell, J. W., Y. Kushnir, G. Ottersen, and M. Visbeck (2003), The North Atlantic oscillation: Climatic significance and environmental impact, *Geophys. Monogr. Ser.*, *134*, 279 pp.
Iglesias, A., L. Garrote, F. Flores, and M. Moneo (2007), Challenges to manage the risk of water scarcity and climate change in the Mediterranean, *Water Resour. Manage.*, *21*(5), 775–788.
Ionita, M., G. Lohmann, and N. Rimbu (2008), Prediction of spring Elbe discharge based on stable teleconnections with winter global temperature and precipitation, *J. Clim.*, *21*, 6215–6226.
Ionita, M., G. Lohmann, N. Rimbu, and S. Chelcea (2011), Interannual variability of Rhine River streamflow and its relationship with large-scale anomaly patterns in Spring and Autumn, *J. Hydrometeorol.*, *13*(1), 172–188.
Izumo, T., J. Vialard, M. Lengaigne, C. de Boyer Montegut, S. K. Behera, J.-J. Luo, S. Cravatte, S. Masson, and T. Yamagata (2010), Influence of the state of the Indian Ocean Dipole on the following year/'s El Nino, *Nat. Geosci.*, *3*(3), 168–172.
Jolliffe, I. T., and D. B. Stephenson (2003), *Forecast Verification: A Practitioner's Guide in Atmospheric Sciences*, Chapter 1. Introduction, pp. 1–11, John Wiley.
Kalra, A., W. P. Miller, K. W. Lamb, S. Ahmad, and T. Piechota (2013), Using large-scale climatic patterns for improving long lead time streamflow forecasts for Gunnison and San Juan River Basins, *Hydrol. Processes*, *27*(11), 1543–1559.
Knippertz, P., U. Ulbrich, F. Marques, and J. Corte-Real (2003), Decadal changes in the link between El Niño and springtime North Atlantic oscillation and European–North African rainfall, *Int. J. Climatol.*, *23*(11), 1293–1311.
Krichak, S. O., P. Kishcha, and P. Alpert (2002), Decadal trends of main Eurasian oscillations and the Eastern Mediterranean precipitation, *Theor. Appl. Climatol.*, *72*(3-4), 209–220.
Kroll, C. N., and P. Song (2013), Impact of multicollinearity on small sample hydrologic regression models, *Water Resour. Res.*, *49*, 3756–3769, doi:10.1002/wrcr.20315.
Kundzewicz, Z. W., and A. J. Robson (2004), Change detection in hydrological records, *Hydrol. Sci. J.*, *49*(1), 7–19.
Lamb, K., T. Piechota, O. Aziz, and G. Tootle (2010), Basis for extending long-term streamflow forecasts in the Colorado River Basin, *J. Hydrol. Eng.*, *16*(12), 1000–1008.
Lilliefors, H. W. (1967), On the Kolmogorov-Smirnov test for normality with mean and variance unknown, *J. Am. Stat. Assoc.*, *62*, 399–402.
Linkin, M. E., and S. Nigam (2008), The North Pacific oscillation-West Pacific teleconnection pattern: Mature-phase structure and winter impacts, *J. Clim.*, *21*(9), 1979–1997.
Lopez-Bustins, J.-A., J. Martin-Vide, and A. Sánchez-Lorenzo (2008), Iberia winter rainfall trends based upon changes in teleconnection and circulation patterns, *Global Planet. Change*, *63*(2–3), 171–176.
López-Moreno, J. I., S. Beguería, S. M. Vicente-Serrano, and J. M. García-Ruiz (2007), Influence of the North Atlantic Oscillation on water resources in central Iberia: Precipitation, streamflow anomalies, and reservoir management strategies, *Water Resour. Res.*, *43*, W09411, doi:10.1029/2007WR005864.
López-Moreno, J. I., S. M. Vicente-Serrano, S. Beguería, J. M. García-Ruiz, M. M. Portela, and A. B. Almeida (2009), Dam effects on droughts magnitude and duration in a transboundary basin: The Lower River Tagus, Spain and Portugal, *Water Resour. Res.*, *45*, W02405, doi:10.1029/2008WR007198.
Lorenzo, M. N., J. J. Taboada, I. Iglesias, and M. Gómez-Gesteira (2010), Predictability of the spring rainfall in Northwestern Iberian Peninsula from sea surfaces temperature of ENSO areas, *Clim. Change*, *107*(3-4), 329–341.
Lorenzo-Lacruz, J., S. M. Vicente-Serrano, J. I. López-Moreno, S. Beguería, J. M. García-Ruiz, and J. M. Cuadrat (2010), The impact of droughts and water management on various hydrological systems in the headwaters of the Tagus River (central Spain), *J. Hydrol.*, *386*(1–4), 13–26.
Lorenzo-Lacruz, J., S. M. Vicente-Serrano, J. I. López-Moreno, J. C. González-Hidalgo, and E. Morán-Tejeda (2011), The response of Iberian rivers to the North Atlantic oscillation, *Hydrol. Earth Syst. Sci.*, *15*(8), 2581–2597.
Lorenzo-Lacruz, J., E. Morán-Tejeda, S. M. Vicente-Serrano, and J. I. López-Moreno (2013a), Streamflow droughts in the Iberian Peninsula between 1945 and 2005: Spatial and temporal patterns, *Hydrol. Earth Syst. Sci.*, *17*(1), 119–134.

Lorenzo-Lacruz, J., S. M. Vicente-Serrano, J. C. González-Hidalgo, J. I. López-Moreno, and N. Cortesi (2013b), Hydrological drought response to meteorological drought in the Iberian Peninsula, *Clim. Res.*, *58*, 117–131.
Mariotti, A., N. Zeng, and K. M. Lau (2002), Euro-Mediterranean rainfall and ENSO: A seasonally varying relationship, *Geophys. Res. Lett.*, *29*(12), 1621, doi:10.1029/2001GL014248.
Martin-Vide, J., and J. A. Lopez-Bustins (2006), The western Mediterranean oscillation and rainfall in the Iberian Peninsula, *Int. J. Climatol.*, *1475*(11), 1455–1475.
Martin-Vide, J., A. Sanchez-Lorenzo, J. A. Lopez-Bustins, M. J. Cordobilla, A. Garcia-Manuel, and J. M. Raso (2008), Torrential rainfall in north-east of the Iberian Peninsula: Synoptic patterns and WeMO influence, *Adv. Sci. Res.*, *2*, 99–105.
Matsumura, S., X. Zhang, and K. Yamazaki (2014), Summer Arctic atmospheric circulation response to spring Eurasian snow cover and its possible linkage to accelerated sea ice decrease, *J. Clim.*, *27*(17), 6551–6558.
Mestas-Nunez, A. M., and D. B. Enfield (2001), Eastern equatorial Pacific SST variability: ENSO and Non-ENSO components and their climatic associations. *J. Clim.*, *14*, 391–402.
Morán-Tejeda, E., J. I. López Moreno, A. Ceballos-Barbancho, and S. Vicente-Serrano, (2011), Evaluating Duero's basin (Spain) response to the NAO phases: Spatial and seasonal variability, *Hydrol. Processes*, *25*(8), 1313–1326.
Ogi, M., and K. Yamazaki (2010), Trends in the summer northern annular mode and Arctic sea ice, *Sola*, *6*, 41–44.
Orsolini, Y. J., and N. G. Kvamstø (2009), Role of Eurasian snow cover in wintertime circulation: Decadal simulations forced with satellite observations, *J. Geophys. Res.*, *114*, D19108, doi:10.1029/2009JD012253.
Oubeidillah, A. A., G. A. Tootle, C. Moser, T. Piechota, and K. Lamb (2011), Upper Colorado River and Great Basin streamflow and snowpack forecasting using Pacific oceanic-atmospheric variability, *J. Hydrol.*, *410*(3), 169–177.
Outten, S. D., and I. Esau (2012), A link between Arctic sea ice and recent cooling trends over Eurasia, *Clim. Change*, *110*(3–4), 1069–1075.
Overland, J. E., and M. Wang (2010), Large-scale atmospheric circulation changes are associated with the recent loss of Arctic sea ice, *Tellus Ser. A*, *62*(1), 1–9.
Paredes, D., R. M. Trigo, R. Garcia-Herrera, and I. Franco Trigo (2006), Understanding precipitation changes in Iberia in early spring: Weather typing and storm-tracking approaches, *J. Hydrometeorol.*, *7*, 101–113.
Park, S. (2004), Remote ENSO influence on Mediterranean sky conditions during late summer and autumn: Evidence for a slowly evolving atmospheric bridge, *Q. J. R. Meteorol. Soc.*, *130*(602), 2409–2422.
Peings, Y., and G. Magnusdottir (2013), Response of the wintertime northern hemisphere atmospheric circulation to current and projected Arctic Sea ice decline: A numerical study with CAM5, *J. Clim.*, *27*(1), 244–264.
Peings, Y., E. Brun, V. Mauvais, and H. Douville (2013), How stationary is the relationship between Siberian snow and Arctic Oscillation over the 20th century?, *Geophys. Res. Lett.*, *40*, 183–188, doi:10.1029/2012GL054083.
Pettitt, A. N. (1979), A non-parametric approach to the change-point problem, *J. Appl. Stat.*, *28*(2), 126–135.
Piechota, T., F. Chiew, J. Dracup, and T. McMahon (2001), Development of exceedance probability streamflow forecast, *J. Hydrol. Eng.*, *6*(1), 20–28.
Pozo-Vázquez, D., S. R. Gámiz-Fortis, J. Tovar-Pescador, M. J. Esteban-Parra, and Y. Castro-Díez (2005), El Niño-Southern Oscillation events and associated European winter precipitation anomalies, *Int. J. Climatol.*, *25*(1), 17–31.
Quadrelli, R., and J. M. Wallace (2004), A simplified linear framework for interpreting patterns of northern hemisphere wintertime climate variability, *J. Clim.*, *17*(19), 3728–3744.
Rimbu, N., C. Boroneant, C. Buta, and M. Dima (2002), Decadal variability of the Danube river flow in the lower basin and its relation with the North Atlantic oscillation, *Int. J. Climatol.*, *22*(10), 1169–1179.
Rinke, A., K. Dethloff, W. Dorn, D. Handorf, and J. C. Moore (2013), Simulated Arctic atmospheric feedbacks associated with late summer sea ice anomalies, *J. Geophys. Res. Atmos.*, *118*(14), 7698–7714, doi:10.1002/jgrd.50584.
Rodó, X., E. Baert, and F. A. Comín (1997), Variations in seasonal rainfall in Southern Europe during the present century: Relationships with the North Atlantic oscillation and the El Niño-Southern oscillation, *Clim. Dyn.*, *13*(4), 275–284.
Rodriguez-Puebla, C., a. H. Encinas, and J. Sáenz (2001), Winter precipitation over the Iberian peninsula and its relationship to circulation indices, *Hydrol. Earth Syst. Sci.*, *5*(2), 233–244.
Sáenz, J., C. Rodríguez-Puebla, J. Fernández, and J. Zubillaga (2001), Interpretation of interannual winter temperature variations over south-western Europe, *J. Geophys. Res.*, *106*(20), 641–652.
Saito, K., and J. Cohen (2003), The potential role of snow cover in forcing interannual variability of the major Northern hemisphere mode, *Geophys. Res. Lett.*, *30*(6), 1302, doi:10.1029/2002GL016341.
Sánchez-Gómez, E., S. Somot, and A. Mariotti (2009), Future changes in the Mediterranean water budget projected by an ensemble of regional climate models, *Geophys. Res. Lett.*, *36*, L21401, doi:10.1029/2009GL040120.
Schneider, U., A. Becker, P. Finger, A. Meyer-Christoffer, M. Ziese, and B. Rudolf (2013), GPCC's new land surface precipitation climatology based on quality-controlled in situ data and its role in quantifying the global water cycle, *Theor. Appl. Climatol.*, *115*(1–2), 15–40, doi: 10.1007/s00704-013-0860-x.
Serrano, A., J. A. García, V. L. Mateos, M. L. Cancillo, and J. Garrido (1999), Monthly modes of variation of precipitation over the Iberian Peninsula, *J. Clim.*, *12*(9), 2894–2919.
Serrano, A., J. A. García, V. L. Mateos, M. L. Cancillo, and J. Garrido (1999), Monthly modes of variation of precipitation over the Iberian Peninsula, *J. Clim.*, *12*(9), 2894–2919.
Sittichok, K., A. Gado Djibo, O. Seidou, H. Moussa Saley, H. Karambiri, and J. Paturel (2014), Statistical seasonal rainfall and streamflow forecasting for the Sirba watershed, West Africa, using sea surface temperatures, *Hydrol. Sci. J.*, doi:10.1080/02626667.2014.944526.
Shaman, J., and E. Tziperman (2011), An atmospheric teleconnection linking ENSO and southwestern European precipitation, *J. Clim.*, *24*(1), 124–139.
Sordo, C., M. D. Frías, S. Herrera, A. S. Cofiño, and J. M. Gutiérrez (2008), Interval-based statistical validation of operational seasonal forecasts in Spain conditioned to El Niño–Southern Oscillation events, *J. Geophys. Res.*, *113*, D17121, doi:10.1029/2007JD009536.
Tang, C., T. C. Piechota, and D. Chen (2011), Relationships between oceanic and atmospheric patterns and soil moisture in the Upper Colorado River Basin, *J. Hydrol.*, *411*(1), 77–90.
Tomita, T., B. Wang, T. Yasunari, and H. Nakamura (2001), Global patterns of decadal-scale variability observed in sea surface temperature and lower-tropospheric circulation fields, *J. Geophys. Res. Oceans*, *106*(C11), 26805–26815.
Tootle, G. A., T. C. Piechota, and F. Gutiérrez (2008), The relationships between Pacific and Atlantic Ocean sea surface temperatures and Colombian streamflow variability, *J. Hydrol.*, *349*(3-4), 268–276.
Trigo, R. M., and J. P. Palutikof (2001), Precipitation scenarios over Iberia: A comparison between direct GCM output and different down-scaling techniques, *J. Clim.*, *14*, 4422–4446.

Trigo, R. M., D. Pozo-Vázquez, T. J. Osborn, Y. Castro-Díez, S. Gámiz-Fortis, and M. J. Esteban-Parra (2004), North Atlantic oscillation influence on precipitation, river flow and water resources in the Iberian Peninsula, *Int. J. Climatol.*, *24*(8), 925–944.

Vicente-Serrano, S. M. (2006), Differences in spatial patterns of drought on different time scales: An analysis of the Iberian Peninsula, *Water Resour. Manage.*, *20*(1), 37–60.

Vicente-Serrano, S. M., and J. I. López-Moreno (2005), Hydrological response to different time scales of climatological drought: An evaluation of the Standardized Precipitation Index in a mountainous Mediterranean basin, *Hydrol. Earth Syst. Sci.*, *9*(5), 523–533.

Vicente-Serrano, S., J. López-Moreno, S. Beguería, J. Lorenzo-Lacruz, C. Azorin-Molina, and E. Morán-Tejeda (2011), Accurate computation of a streamflow drought index, *J. Hydrol. Eng.*, *17*(2), 318–332.

Vicente-Serrano, S. M., et al. (2014), Evidence of increasing drought severity caused by temperature rise in southern Europe, *Environ. Res. Lett.*, *9*(4), 044001.

Vihma, T. (2014), Effects of Arctic sea ice decline on weather and climate: A review, *Surv. Geophys.*, *35*(5), 1175–1214.

von Storch, H., and F. W. Zwiers (1999), *Statistical analysis in climate research*, 484 pp., Cambridge Univ. Press, Cambridge, U. K.

Xoplaki, E., J. F. González-Rouco, J. Luterbacher, and H. Wanner (2004), Wet season Mediterranean precipitation variability: Influence of large-scale dynamics and trends, *Clim. Dyn.*, *23*(1), 63–78.

Yu, J.-Y., and S. T. Kim (2010), Relationships between extratropical sea level pressure variations and the Central Pacific and Eastern Pacific types of ENSO, *J. Clim.*, *24*(3), 708–720.

Zuur, A. F., E. N. Ieno, and C. S. Elphick (2010), A protocol for data exploration to avoid common statistical problems, *Methods Ecol. Evol.*, *1*(1), 3–14.